Journal Pre-proof

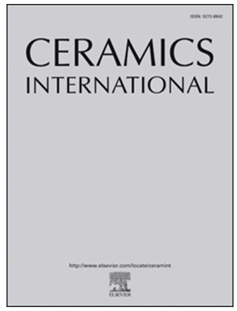

Effect of recycled polymer fibre on dynamic compressive behaviour of engineered geopolymer composites

Hui Zhong, Mingzhong Zhang

PII: S0272-8842(22)01576-0

DOI: https://doi.org/10.1016/j.ceramint.2022.05.023

Reference: CERI 32633

To appear in: *Ceramics International*

Received Date: 18 March 2022

Revised Date: 24 April 2022

Accepted Date: 2 May 2022

Please cite this article as: H. Zhong, M. Zhang, Effect of recycled polymer fibre on dynamic compressive behaviour of engineered geopolymer composites, *Ceramics International* (2022), doi: https://doi.org/10.1016/j.ceramint.2022.05.023.

Effect of recycled polymer fibre on dynamic compressive behaviour of engineered geopolymer composites

Hui Zhong, Mingzhong Zhang[*]

Department of Civil, Environmental and Geomatic Engineering, University College London, London, WC1E 6BT, UK

Abstract: To enhance the cost-effectiveness and sustainability of engineered geopolymer composites (EGC), polyvinyl alcohol (PVA) fibres in EGC can be partially replaced with recycled tyre polymer (RTP) fibres. This paper presents a systematic experimental study on the effects of PVA fibre volume fraction (1.0%, 1.5% and 2.0%) and RTP fibre content (0.25%, 0.5%, 0.75% and 1.0%) on the dynamic compressive behaviour of EGC under various strain rates (54.43-164.13 s^{-1}). Results indicate that the flowability, quasi-static compressive strength and elastic modulus of EGC reduce with the increase of PVA fibre content, where the reductions can be effectively mitigated by adding RTP fibres. The dynamic compressive properties of all investigated mixtures including dynamic compressive strength, dynamic increase factor (DIF) and energy absorption capacity show a pronounced strain rate dependency which can be well described using the proposed equations for DIF against strain rate ranging from 10^{-5} s^{-1} to 10^{3} s^{-1} with R^2 values of mostly greater than 0.9. The dynamic compressive properties of EGC are enhanced with the increasing PVA fibre dosage under various strain rates while replacing PVA fibre with a certain amount of RTP fibre (0.25% and 0.5%) can result in better dynamic compressive properties compared to EGC with 2.0% PVA fibre. EGC containing 1.75% PVA fibre and 0.25% RTP fibre can be considered as the optimal mixture given its superior quasi-static and dynamic compressive properties in comparison with EGC with 2.0% PVA fibre.

Keywords: Strain hardening geopolymer composites; Recycled fibre; Split Hopkinson pressure bar (SHPB); Strain hardening behaviour; Dynamic increase factor; Toughening mechanism

1. Introduction

To mitigate the low brittleness and improve the tensile strength of traditional concrete, a special class of fibre reinforced concrete called engineered cementitious composite (ECC) or strain hardening cementitious composite (SHCC) is developed in the 1990s, which exhibits extraordinary ductility under quasi-static tensile loading accompanied by the formation of multiple microcracks [1]. Nevertheless, the required Portland cement dosage in ECC is generally higher than that for other cementitious composites, which may lower the greenness of ECC given that the production of Portland cement accounts for about 8% of global CO_2 emissions [1-3]. To tackle this issue, one of the emerging solutions is to replace Portland cement with eco-friendly binders, e.g., geopolymers. In recent years, engineered geopolymer composite (EGC) has been increasingly studied, which can be

[*] Corresponding author. E-mail address: mingzhong.zhang@ucl.ac.uk (M. Zhang)

synthesised by a variety of precursors, activators and fibres based on the micromechanical design theory of ECC [1].

Among all types of developed EGC, the ones utilising fly ash [4-7] and ground granulated blast-furnace slag [8-10] as binders have been extensively investigated primarily because of the large availability of them around the world [11, 12]. However, heat curing is typically required for fly ash-based EGC and slag-based EGC has poor workability, short setting time and high shrinkage. These issues may impede the engineering applications of the composites, especially cast-in-situ works [13, 14]. Hence, EGC containing blended fly ash and slag cured at ambient temperature has been attracting increasing attention as it exhibits desired fresh properties and superior tensile behaviour, regardless of the used activators and fibres [13, 15-22]. The existing studies on fly ash-slag based EGC mainly focused on the effects of different factors such as fly ash/slag ratio, silicate modulus of activator, sand content, fibre content, fibre length, curing regime and curing age on the fresh and quasi-static mechanical properties. For instance, fly ash-slag based EGC under ambient temperature curing was found to possess similar tensile properties compared to heat-cured EGC, which can exhibit a tensile strength of 4.6 MPa along with a high tensile strain capacity of 4.2% and can reduce carbon emission and energy consumption by 76% and 36%, respectively in comparison with traditional ECC [13]. The developed fly ash-slag based EGC generally exhibited a tensile strength of 3.06-5.77 MPa, a tensile strain capacity of 2.27-5.81% and tensile crack widths ranging from 28.4-147.34 μm [18-20, 22], which are comparable or even better than traditional ECC [23]. It is worth mentioning that most aforementioned studies have adopted either polyvinyl alcohol (PVA) or polyethylene (PE) fibres to reinforce the geopolymer matrix because of the excellent fibre-matrix bonding for PVA fibres and high tensile strength of PE fibres [7, 22]. However, these fibres have relatively higher material costs than other types of fibre, e.g., steel and polypropylene fibres [24, 25]. In addition, the environmental impact associated with the production of virgin synthetic fibres is inevitable [26]. Thus, it is vital to find and utilise other low cost and sustainable fibres for the development of EGC.

Among all possible attempts, using recycled fibres from natural and synthetic materials (e.g., waste bottles and end-of-life tyres) to develop EGC is a potential solution as it can not only improve the cost-effectiveness and sustainability of EGC but also reduce the solid wastes by turning them into value-added construction ingredients/materials [26-28]. In our previous studies [15, 17], the feasibility of using recycled tyre steel and polymer fibres in EGC was explored, aiming to find an effective disposal way for the large quantity of annually generated waste tyres (around 1500 million [29]). The utilisation of recycled tyre steel (RTS) fibres can offer benefits to the compressive strength and drying shrinkage resistance of EGC while the flexural performance including flexural strength and toughness was weakened [15]. On the other hand, due to the high strength and stiffness of RTS fibres, the flexural crack widths of EGC containing hybrid PVA and RTS fibres were much smaller compared to that of mono-PVA fibre reinforced EGC (mostly less than 60 μm). The tight crack widths may be favourable for durability and self-healing behaviour [30]. Apart from RTS fibres, the feasibility of partially replacing PVA fibres with recycled tyre polymer (RTP) fibres was also studied [17], with a special focus on the uniaxial tensile behaviour, indicating that the presence of RTP fibres weakened the tensile behaviour of mono-PVA fibre reinforced EGC (see Fig. 1), which can be attributed to the reduced fibre bridging effect induced by the low strength and hydrophobic characteristic of RTP fibres. However, the drying shrinkage, material cost and embodied energy of hybrid fibre reinforced EGC were found to be about 17.33%, 34.52% and 16.23% lower than those of mono-PVA fibre reinforced EGC. The influence of recycled tyre fibres on quasi-static mechanical properties of EGC has been preliminarily assessed, while the effect of them on dynamic mechanical properties remains unclear and requires further research, given that concrete structures may be subjected to static loadings as well as dynamic loadings with various strain rates.

So far, the dynamic mechanical properties of EGC have been very rarely studied. It was reported that the tensile failure mode of ambient-cured EGC changed to brittle when the strain rate increased from 10^{-4} s^{-1} to 0.51 s^{-1} while the heat-cured EGC did not show such a phenomenon [22]. Furthermore, fly ash-slag based EGC presented better tensile properties than both fly ash-based and slag-based EGC under quasi-static and dynamic loadings. The EGC mixture containing 2.0% ultra-high-molecular-weight PE fibres demonstrated superior dynamic mechanical properties in terms of tensile strength and energy absorption capacity compared to PVA fibre reinforced EGC and normal-strength ECC [31], which is consistent with the findings presented in Refs. [32, 33] that EGC showed a better impact resistance than ECC at both ambient temperature and elevated temperature (50-150 °C). Besides, the impact resistance of EGC was improved with the increasing molarity of sodium hydroxide up to 12 M [32]. Although the mechanical properties of PVA and PE fibre reinforced EGC under dynamic tensile and drop weight impact loadings have been studied, to the authors' best knowledge, the effects of RTP fibre dosage and strain rate (10^1 to 10^3 s^{-1}) on the dynamic compressive behaviour of fly ash-slag based EGC cured at ambient temperature have not been explored to date, which would hinder the widespread application of such sustainable composites.

The main purpose of this study is to conduct a systematic experimental study on the effects of PVA fibre volume fraction (1.0%, 1.5% and 2.0%) and RTP fibre replacement level of PVA fibre (0.25, 0.5%, 0.75% and 1.0% by volume) on the quasi-static and dynamic compressive behaviour of fly ash-slag based EGC cured at ambient temperature under various strain rates (50-160 s^{-1}). A series of tests were carried out to measure the flowability, quasi-static compressive strength and elastic modulus as well as dynamic compressive properties using split Hopkinson pressure bar (SHPB) in terms of stress-strain response, failure pattern, dynamic compressive strength, dynamic increase factor (DIF) and energy absorption capacity. Based on the obtained experimental data, the empirical equations for DIF were then proposed for all studied mixtures within the considered strain rate range from 10^{-5} s^{-1} to 10^3 s^{-1}, which are crucial and helpful for the structural design. Afterwards, the fibre morphology across the cracking interface after SHPB tests was characterised using the digital microscope and scanning electron microscopy (SEM), based on which the underlying mechanisms of the synergistic effects of hybrid PVA and RTP fibres on the dynamic compressive behaviour of EGC were analysed and discussed in depth.

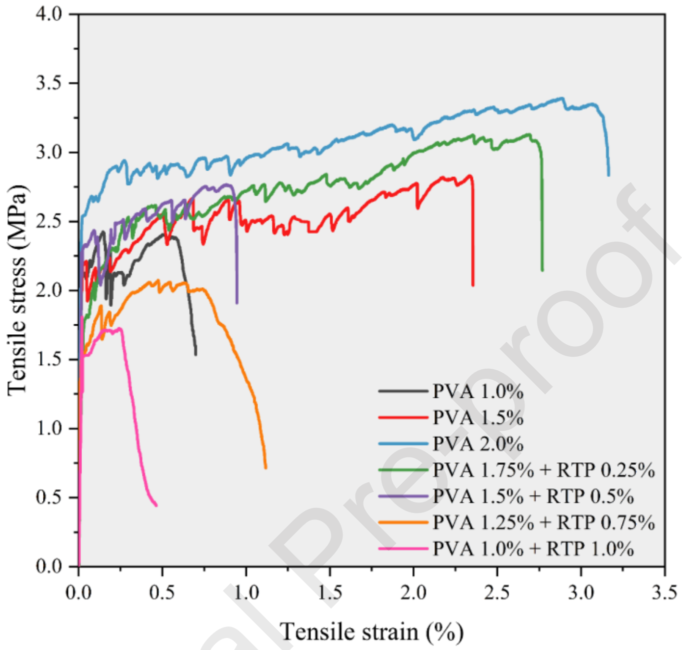

Fig. 1. Uniaxial tensile stress-strain curves of engineered geopolymer composites (EGC) containing various polyvinyl alcohol (PVA) and recycled tyre polymer (RTP) fibre contents [17].

2. Experimental program

2.1. Raw materials

The solid precursors adopted in this study were low calcium fly ash according to ASTM C618-17a [34] and ground granulated blast-furnace slag, the chemical composition and particle size distribution of which are illustrated in Table 1 and Fig. 2a, respectively. Regarding the morphology, fly ash particles are mostly spherical (Fig. 2b) while slag contains a large number of angular particles (Fig. 2c). Fig. 3 illustrates the X-ray diffraction (XRD) patterns of fly ash and slag measured using a Malvern Panalytical X'Pert[3] Powder diffractometer, where $CuK\alpha$ X-ray was employed at 45 kV and 40 mA and 2θ configuration ranging from 5-70^o was applied. It can be observed that fly ash consists of a considerable amount of amorphous phases (board hump range of 2θ=15^o-35^o in Fig. 3) and its major crystalline phases are mullite and quartz. A significant amount of amorphous phases can also be detected for slag, as seen in the board hump from 2θ=25^o to 2θ=35^o in Fig. 3. Fine silica sand was used as aggregate, the particle size distribution of which is presented in Fig. 2a. A combination of sodium hydroxide (SH) solution with a molarity of 10 M and sodium silicate (SS) solution with a silicate modulus (SiO_2/Na_2O) of 3.15 was used as the alkaline activator. A polycarboxylate-based superplasticiser (Sika®ViscoFlow®3000) was applied to control the workability of mixtures. Fig. 4 illustrates the physical appearance of the fibres used in this study including PVA fibres (Kuraray Co., Ltd., Japan) and RTP fibres recycled from the truck tyres, the main properties of which are presented in Table 2. RTP fibres were cleaned before the usage to remove most of the attached rubber particles, the detailed process of which can be found in Ref. [35]. Based on the SEM images of PVA and RTP fibres (Fig. 4a and b), the dimensions of PVA fibres were unified while RTP fibres exhibit irregularity in dimension. The primary composition and main properties of RTP fibres were characterised and reported in a previous study [17].

Table 1 Chemical compositions (wt.%) of fly ash and ground granulated blast-furnace slag.

Oxide	SiO_2	Al_2O_3	Fe_2O_3	CaO	SO_3	MgO	TiO_2	P_2O_5	LOI
Fly ash	57.02	32.35	3.01	2.88	0.41	0.58	1.26	0.20	2.45
Slag	31.85	17.31	0.34	41.20	1.78	6.13	0.62	0.02	0.39

Note: LOI (Loss on Ignition).

Table 2 Main properties of polyvinyl alcohol (PVA) and recycled tyre polymer (RTP) fibres used in this study.

Fibre type	Length (mm)	Diameter (μm)	Tensile strength (MPa)	Elastic modulus (Ga)	Density (kg/m^3)
PVA	12.0	40.0	1560	41.0	1300
RTP	5.2 (2.4)	21.4 (4.4)	761 (115)	3.8 (0.7)	1476 (3)

Note: the values are standard deviations in parentheses.

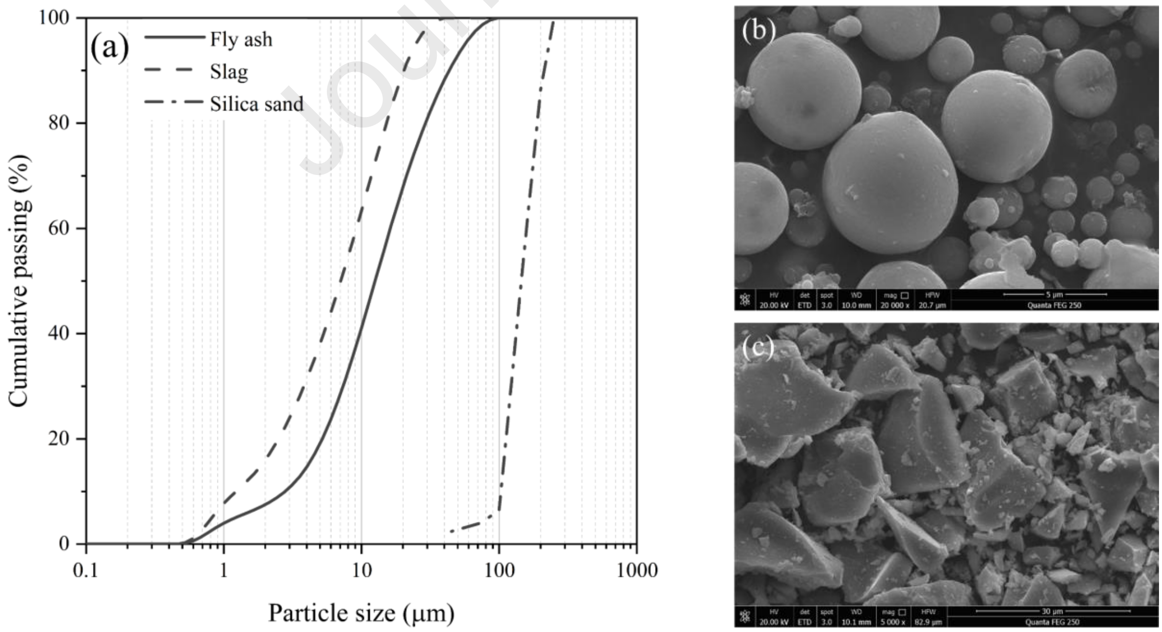

Fig. 2. (a) Particle size distribution of fly ash, slag and silica sand; SEM images of (b) fly ash and (c) slag.

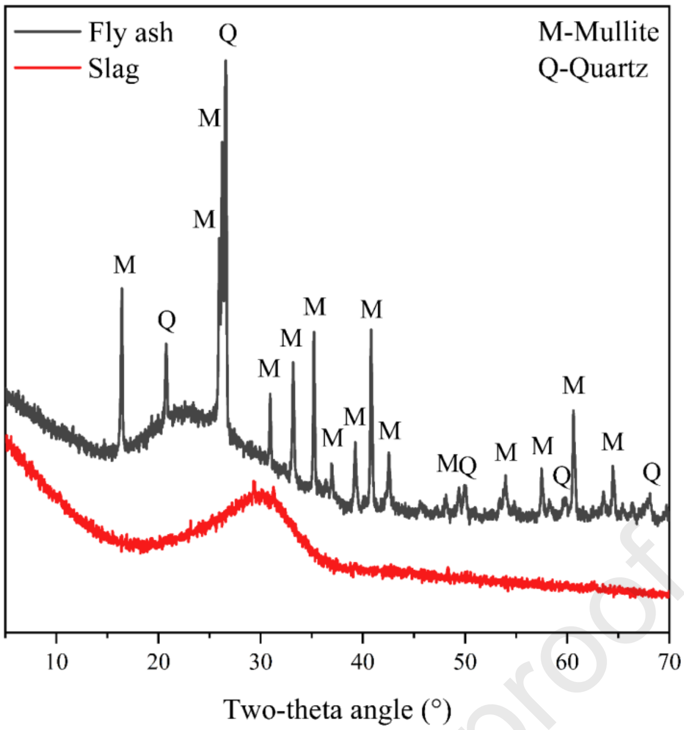

Fig. 3. X-ray diffraction (XRD) patterns of fly ash and slag.

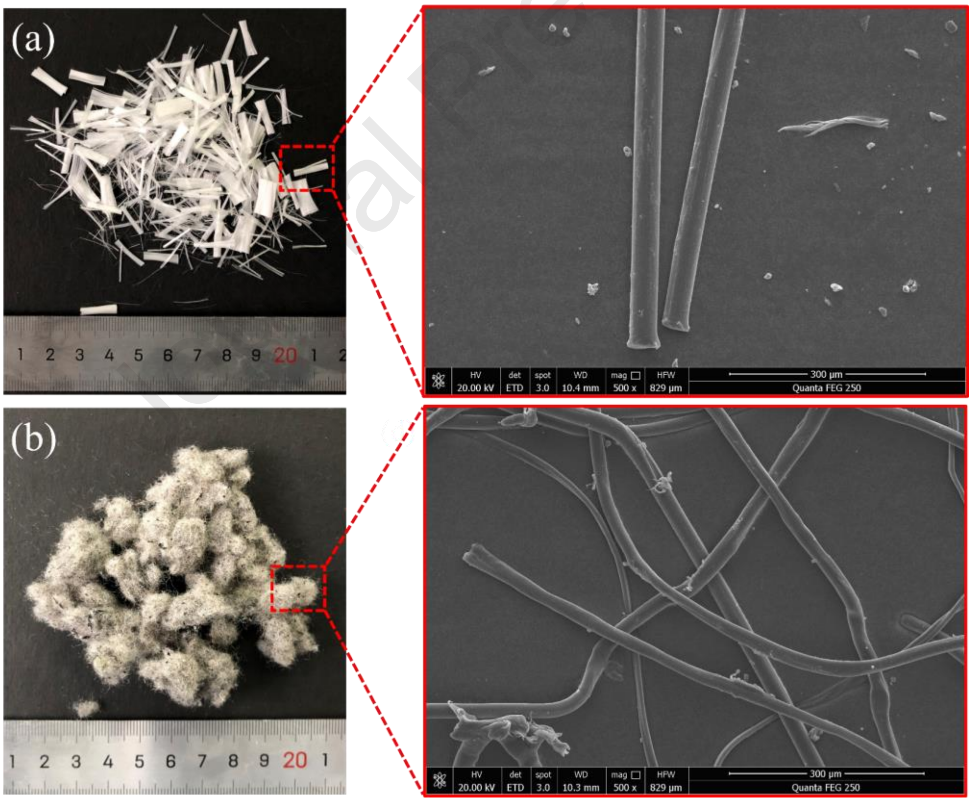

Fig. 4. Images of (a) PVA and (b) RTP fibres.

2.2. Mix proportions

The mix proportions of all studied mixtures are listed in Table 3, which are kept consistent with a previous study [17]. For all mixtures, the weight ratios of fly ash/slag, silica sand/binder, alkaline activator/binder, SS/SH and superplasticiser/binder were set as 4.0, 0.2, 0.45, 1.5 and 0.01 and kept constant. These parameters were selected based on previous studies [14, 16, 21], which can provide acceptable workability and mechanical properties for the geopolymer matrix. The influencing parameters studied here included fibre type (PVA and RTP) and fibre content (0-2.0% by volume). Regarding the meaning of the labels shown in Table 3, for instance, P0R0 denotes the mixture without fibres, while P1.0R1.0 represents the mixture reinforced with two types of fibres where ‘P1.0’ indicates the content of PVA fibre (1.0%) and ‘R1.0’ denotes the dosage of RTP fibre (1.0%). These mixtures were designed to examine the effects of PVA fibre content as well as RTP fibre addition and replacement on the quasi-static and dynamic mechanical properties of EGC.

Table 3 Mix proportions of all studied mixtures.

Mixture label	By weight					By volume (%)	
	Binder		Silica sand*	Alkaline activator*	SP*	PVA fibre	RTP fibre
	Fly ash	Slag					
P0R0	0.8	0.2	0.2	0.45	0.01	0	0
P1.0R0						1.0	0
P1.5R0						1.5	0
P2.0R0						2.0	0
P1.75R0.25						1.75	0.25
P1.5R0.5						1.5	0.5
P1.25R0.75						1.25	0.75
P1.0R1.0						1.0	1.0

Note: *weight ratio of binder; SP (superplasticiser).

2.3. Sample preparation

The SH solution was prepared by dissolving SH pellets (>99% purity) in the tap water for 24 h before the mixture preparation. The mixing process for mono-PVA fibre reinforced EGC is consistent with that given in Ref. [17]: (1) add fly ash, slag, silica sand and mix for 90 s; (2) add alkaline activator and mix for 180 s; (3) add superplasticiser; (4) add PVA fibres slowly. Regarding the mixtures containing hybrid PVA and RTP fibres, the RTP fibres were first mixed with a small amount of alkaline activator, which can effectively avoid the fibre clumping or balling as per previous studies [17, 36, 37]. The mixing process of all EGC mixtures lasted about 10 min. The fresh mixtures were poured into cylindrical moulds (Ø 100 mm × 200 mm and Ø 100 mm × 50 mm) in two layers. After casting with sufficient compaction, all mixtures were sealed with the plastic sheet at room temperature (20 ± 2 °C) and then de-moulded after 24 h. Then, all samples were cured in a standard room (20 ± 2 °C, 95% RH) for 28 d. Before the quasi-static and dynamic mechanical tests, the end surfaces of all cylindrical specimens were polished to ensure they are flat and parallel.

2.4. Test methods

2.4.1. Flowability test

The flowability of fresh mixtures was determined using the flow table test as per ASTM C1437-15 [38]. Herein, the fresh mixtures were firstly poured into a truncated conical mould with a top diameter of 70 mm, a bottom diameter of 100 mm and a height of 50 mm. Then, the spread diameter of the tested mixture was measured after lifting the mould and tapping the flow table 25 times. Three repeated tests were conducted for each mixture to determine the flowability that can be calculated as:

$$F = \frac{D_s - D_b}{D_b} \times 100\% \quad (1)$$

where F is the flowability of the tested mixture, D_s is the spread diameter of the tested mixture, and D_b is the bottom diameter of the truncated conical mould (i.e., 100 mm).

2.4.2. Quasi-static compression test

For each mixture, the uniaxial compression test on three cylindrical specimens (Ø 100 mm × 200 mm) according to ASTM C39-21 [39]. The loading rate was set constant as 1.0 mm/min which is equivalent to a strain rate of about 8.33×10^{-5} s^{-1}. The tested specimens had the same diameter as those for the dynamic compression test but with a different aspect ratio (i.e., length/diameter = 2.0). Previous studies [40-42] revealed that the quasi-static compressive strength obtained based on this aspect ratio is more appropriate for calculating DIF as the size and end friction effects can be minimised. Once the average quasi-static compressive strength was obtained, the elastic modulus test was performed following ASTM C469-14 [43]. Fig. 5 shows the setup for the elastic modulus test, where two strain gauges were installed at the mid-height of the tested specimen to measure the longitudinal strain. During the test, the tested specimen was initially loaded to 40% of its ultimate load-carrying capacity based on the average quasi-static compressive strength, followed by an unloading phase and this testing procedure was repeated three times. The corresponding elastic modulus can be calculated as:

$$E_s = \frac{\sigma_2 - \sigma_1}{\varepsilon_2 - 0.00005} \quad (2)$$

where E_s is the elastic modulus of the tested specimen, σ_2 is the stress corresponding to 40% of the ultimate stress, σ_1 is the stress at a longitudinal strain of 50 με, and ε_2 is the longitudinal strain at σ_2.

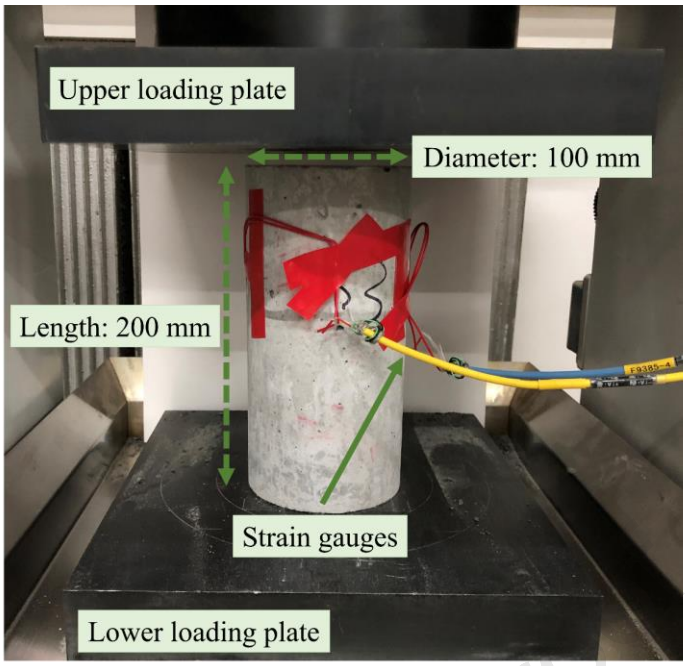

Fig. 5. Test setup for measuring elastic modulus.

2.4.3. Dynamic compression test

The dynamic compressive behaviour of all mixtures was evaluated using a SHPB with a diameter of 100 mm. Fig. 6 presents the schematic illustration of the SHPB testing system, the main components of which include a striker bar (600 mm), an incident bar (5000 mm), a transmission bar (3500 mm) and an absorbing bar (1200 mm) that are all made of high-strength steel materials. The velocity of the striker bar can be adjusted by either varying the pressure level or changing the depth of the striker bar inside the launch tube. In this study, the depth of the striker bar was fixed while the pressure level was altered from 0.4 MPa to 1.0 MPa to generate various impact velocities. Three specimens were used for each pressure level. Before the test, the tested specimen was first sandwiched between the incident bar and the transmission bar. The used specimen had a diameter of 100 mm and a length of 50 mm (aspect ratio: 0.5), which was selected to eliminate the axial inertia effect during the impact loading [42, 44]. Besides, the end surfaces of the specimen were applied with a small amount of grease to minimise the end friction effect. Once the test was started, the striker bar was launched by the immediate release of the compressed nitrogen in the pressure vessel and then it accelerated inside the launch tube until impacting the incident bar, generating an incident wave. When the incident wave reached the interface between the incident bar and the specimen, part of the wave was reflected, and the rest propagated along the transmission bar. The incident strain ($\varepsilon_i(t)$), reflected strain ($\varepsilon_r(t)$) and transmission strain ($\varepsilon_t(t)$) were recorded by the strain gauges.

In this study, the pulse shaping technique was used to ensure the validity of SHPB test results by filtering out the high-frequency components in the incident pulse and achieving the dynamic stress equilibrium [45, 46]. As illustrated in Fig. 6, a small piece of rubber was placed on the impact end of the incident bar, which changed the shape of the incident pulse to extend its rising time for better facilitating the dynamic stress equilibrium [45, 47]. It should be noted that the rising time of the incident pulse can be increased by either reducing the diameter of the pulse shaper or raising its thickness [48]. Thus, trial tests were performed to select the suitable dimension of the pulse shaper. The rubber with a diameter of 30 mm and a thickness of 3 mm was found to be adequate for producing dynamic stress equilibrium, which was similar to those employed by other studies [42, 49]. Fig. 7 presents some examples of checking the dynamic stress equilibrium for plain and EGC mixtures after removing the time lags, indicating that the sum of incident stress and reflected stress fitted well with the transmission stress during the whole loading process, which suggests the achievement of dynamic stress equilibrium condition. Based on the one-dimensional stress wave theory, the time history of stress ($\sigma(t)$), strain ($\varepsilon(t)$) and strain rate ($\dot{\varepsilon}(t)$) can be calculated as [45]:

$$\sigma(t) = \frac{E_b A_b}{2A_s}(\varepsilon_i(t) + \varepsilon_r(t) + \varepsilon_t(t)) \tag{3}$$

$$\varepsilon(t) = \frac{C_b}{l_s}\int_0^t (\varepsilon_i(t) - \varepsilon_r(t) - \varepsilon_t(t))\ dt \tag{4}$$

$$\dot{\varepsilon}(t) = \frac{C_b}{l_s}(\varepsilon_i(t) - \varepsilon_r(t) - \varepsilon_t(t)) \tag{5}$$

where E_b, A_b and C_b denote the elastic modulus, cross-sectional area and longitudinal wave velocity of the SHPB bar, respectively, and A_s and l_s are the cross-sectional area and length of the tested specimen, respectively.

After the SHPB tests, the fibre conditions crossing the crack interfaces were captured using a digital microscope. Besides, to better characterise the fibre morphology in EGC subjected to high-velocity impacts, SEM scanning (FEI, QUANTA FEG 250, USA) was carried out on some fracture pieces of failed specimens.

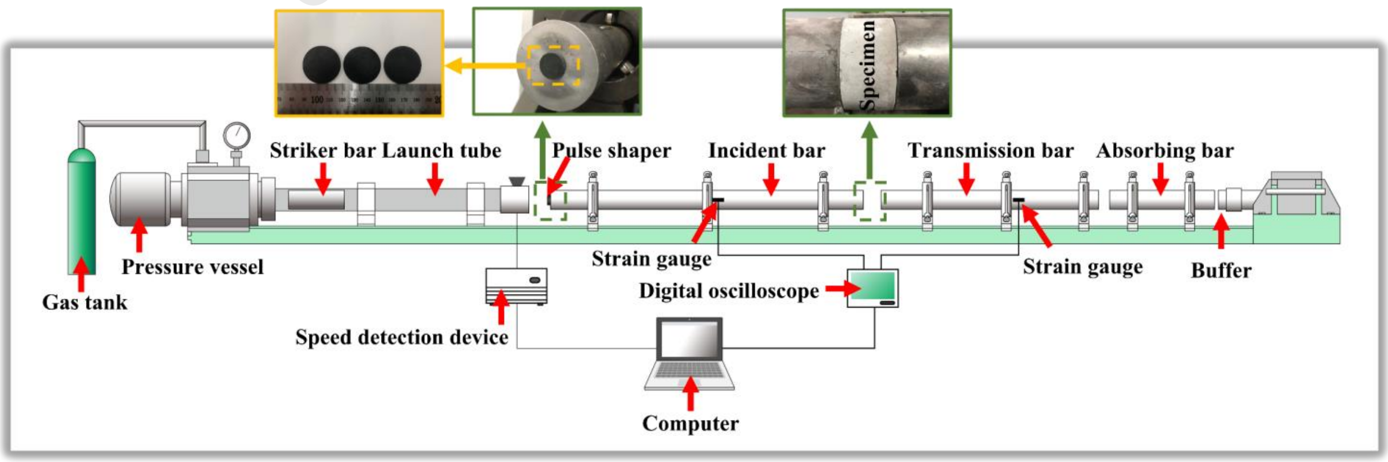

Fig. 6. Schematic illustration of split Hopkinson pressure bar (SHPB) test.

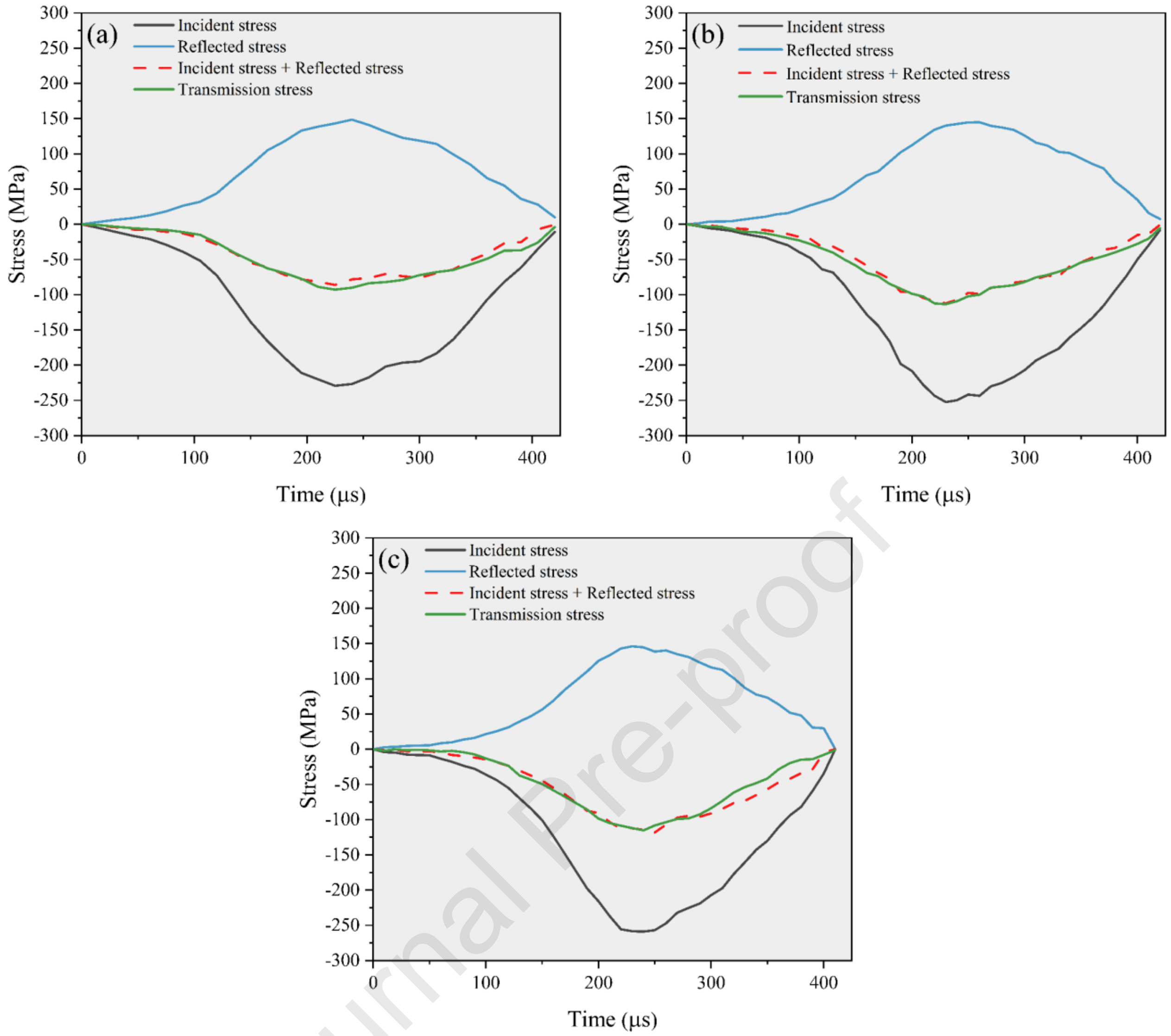

Fig. 7. Examples of typical dynamic stress equilibrium: (a) P0R0 at 139.57 s^{-1}; (b) P2.0R0 at 139.21 s^{-1} and (c) P1.75R0.25 at 143.85 s^{-1}.

3. Results and discussion

3.1. Flowability

Fig. 8 depicts the effects of PVA and RTP fibres on the flowability of EGC. It can be observed that the flowability of mixtures was reduced by 12.14-52.34% compared to that of plain geopolymer mixture when the fibres were added. Fresh mixtures containing fibres were less flowable and more viscous, which may affect the compactness and internal structure especially fibre distribution, impairing the hardened properties of EGC. This can be ascribed to the contact network between fibres and increased liquid content absorption on the surfaces of fibres, leading to increased overall shear resistance [50, 51]. Additionally, the fibre properties and critical fibre dosage can affect the reduction degree of flowability [51]. For instance, it was reported that the flowability of EGC tended to be lower when the fibres had a larger surface area [5] and the fibre balling behaviour would be easier to induce after exceeding the critical fibre content [51]. As seen in Fig. 8, replacing PVA fibre with 0.25% RTP fibre did not significantly reduce the flowability of EGC as compared with P2.0R0 (98% against

95%), which can be partially ascribed to the lower aspect ratio (length/diameter) of RTP fibres [5, 52]. However, the flowability of mixtures containing RTP fibres over 0.25% was about 17.11-24.51% lower in comparison with P2.0R0, suggesting that the critical dosage of RTP fibre for EGC would be in the range of 0.25-0.5% as exceeding this range could increase the possibility of rendering a congested fibre network inside EGC. Therefore, the overall workability of hybrid fibre reinforced EGC can be reduced considerably compared to that of mono-fibre reinforced EGC. Similar findings were also reported in previous studies [53, 54]. It is worth noting that all mixtures had acceptable flowability without obvious fibre balling or clumping behaviour based on visual observations.

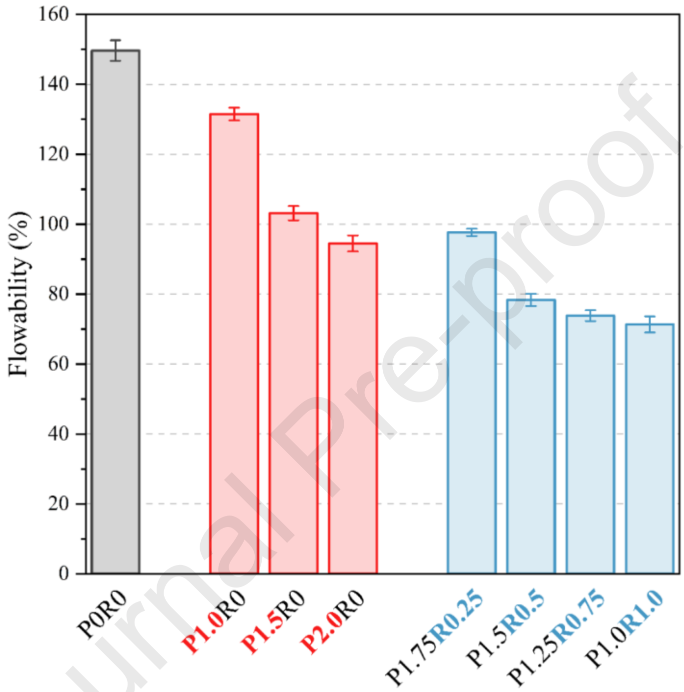

Fig. 8. Effects of PVA and RTP fibres on flowability of EGC.

3.2. Quasi-static compressive strength

Fig. 9a shows the quasi-static compressive strength of all mixtures, which ranged from 45.87 MPa to 52.1 MPa. Similar to previous studies on EGC [15, 17] and ECC [55, 56], the inclusion of PVA fibres did not lead to a positive effect on the compressive strength of composites. For instance, the compressive strengths of P1.0R0, P1.5R0 and P2.0R0 were about 0.45-7.17% lower than that of P0R0. As compared with P2.0R0, incorporating RTP fibres in EGC led to a slightly higher or lower compressive strength while the differences can be considered as insignificant (0.48-5.17%). As mentioned earlier, the reduced flowability caused by the fibre addition can lower the compactness of the composites and thus compressive strength. This can be evidenced that the decreasing trend of compressive strength induced by the fibre addition coincides with that of flowability (Section 3.1). Besides, the used PVA and RTP fibres in this study may entrap a certain amount of air during the mixing which would increase the porosity near the fibres, forming the weak zone inside EGC [51]. The hydrophobic characteristic of RTP fibres can lead to poor fibre-matrix bonding [17] and hence, the compressive strength of EGC tended to be lower at a higher RTP fibre dosage (over 0.5%). It is worth noting that the compressive strength of P1.75R0.25 was slightly higher (about 2.14%) than that of P2.0R0, which can be attributed to its better internal structure such as better fibre distribution, smaller porosity and less defects. The incorporation of either PVA or RTP fibres did not improve the compressive strength of geopolymers but resulted in enhanced ductility. As seen in Fig. 9b, P0R0 showed an hourglass compressive failure shape where some oblique cracks appeared near the end surfaces and splitting cracks can be found in the mid-portion of the specimen due to the pure tensile effect [40], while the presence of fibres retained the original cylindrical shape of the specimen exhibiting a longitudinal main crack accompanied by derivative micro-cracks (Fig. 9c). This can be attributed to the crack-arresting ability of fibres [15, 55, 57]. In general, all EGC mixtures showed adequate compressive strength for basic engineering applications.

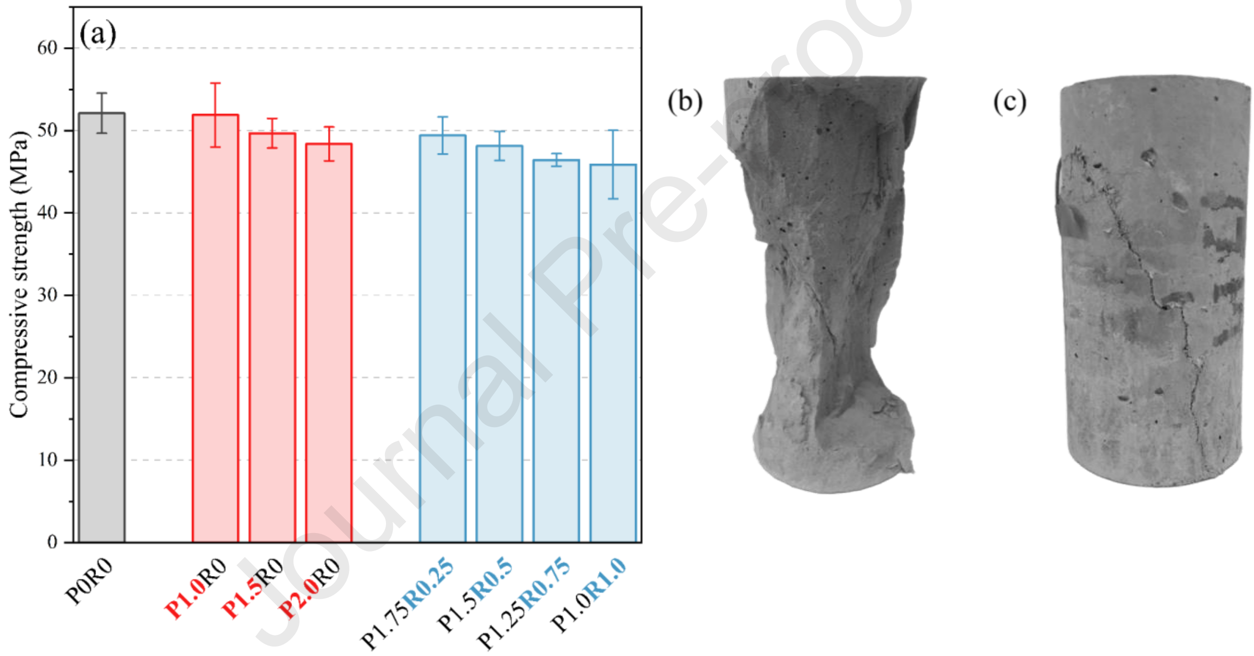

Fig. 9. (a) Quasi-static compressive strength of all mixtures and representative compressive failure modes of (b) plain geopolymer mixture and (c) hybrid PVA and RTP fibre reinforced EGC.

3.3. Elastic modulus

The elastic modulus of materials is defined as the ability to sustain the applied stress for every unit strain within the elastic region, which is strongly associated with the compressive strength. Fig. 10a illustrates the elastic modulus of geopolymers with and without fibres. As observed, P0R0 achieved the highest elastic modulus of 18.33 GPa while by comparison, the elastic modulus of all EGC mixtures was about 14.67-35.78% lower, which agrees well with the tendency of quasi-static compressive strength. Previous studies [58-60] also reported that the incorporation of synthetic fibres reduced the elastic modulus of composites as compared with plain mixtures, which can be mainly ascribed to the internal structure of the composite (e.g., porosity and fibre orientation) as well as the stiffness of incorporated fibres [51]. Given the high stiffness of steel fibres (about 210 GPa), adding a certain amount of steel fibres (1.0-2.0%) into geopolymers can lead to a slight improvement in the elastic modulus [60, 61]. However, as listed in Table 2, PVA and RTP fibres have lower elastic modulus (3.8 GPa and 41 GPa) than steel fibres and thus may partially contribute to the reduced elastic modulus of EGC, while it was reported that fibre stiffness has a minor effect on the mechanical properties of composites before cracking [24]. During the elastic modulus test, no visible cracking appeared on the tested specimen. As discussed above, replacing a small dosage of PVA fibre (0.25%) with RTP fibre led to slightly better workability and quasi-static compressive strength compared to EGC with 2.0% PVA fibre (P2.0R0), implying that the specimen had a better internal structure in terms of lower porosity and better fibre dispersion. Hence, the elastic modulus of P1.75R0.25 was around 25.56% higher than that of P2.0R0. In addition, the elastic modulus of all other hybrid fibre reinforced EGC mixtures was in the range of 11.77-13.79 GPa which was either greater or comparable in comparison with P2.0R0.

Elastic modulus is regarded as an important index for structural designs and hence, it is vital to develop a reliable model of elastic modulus concerning the compressive strength. For comparison, the proposed equations for estimating the elastic modulus of Portland cement concrete [62, 63] and geopolymer concrete [64] were plotted in Fig. 10b, along with some data on geopolymer composites collected from previous studies [57, 60, 65]. It can be seen that the elastic modulus of all geopolymer composites especially EGC mixtures obtained from other studies [57, 65] was significantly lower than the calculated values using the equations for Portland cement and geopolymer concrete, which can be attributed to the absence of coarse aggregates in the geopolymer composites. It suggests that the existing models for predicting the elastic modulus would not be suitable for EGC. However, the available elastic modulus data of EGC is insufficient to offer a reliable model and therefore, more extensive studies are needed considering different grades of compressive strength for EGC.

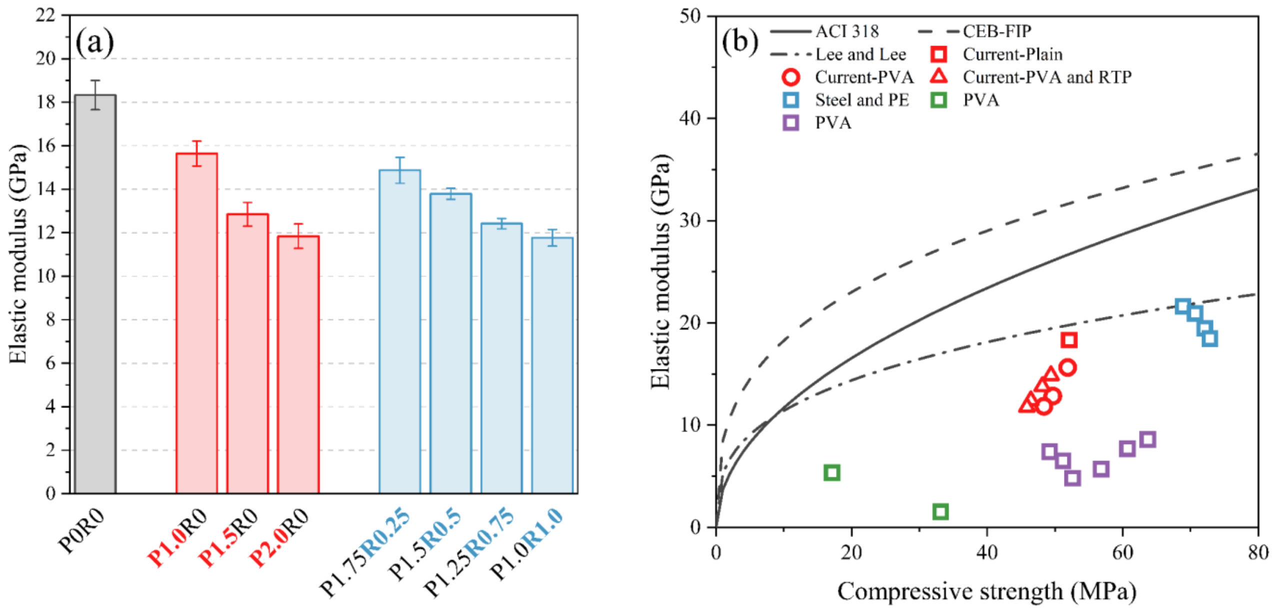

Fig. 10. Elastic modulus: (a) obtained from this study; (b) in comparison with other existing models and studies [57, 60, 62-65].

3.4. Dynamic compressive behaviour

3.4.1. Stress-strain response

The stress-strain response is an important index for characterising the dynamic properties of materials and the representative stress-strain curves of all mixtures covering the strain rates from 54.43 to 164.13 s^{-1} are presented in Fig. 11. As the strain rate of concrete is not constant during the entire process of dynamic loading [41, 66] and the strain rate at the failure point (i.e., peak stress) can be considered as the representative strain rate [67-69], the same approach was employed to define the representative strain rate in this study. As seen, the stress-strain curves of the plain geopolymer mixture and EGC had similar shapes consisting of ascending and descending stages. During the ascending stage, the stress increases linearly with the rising strain within the elastic region followed by the non-linear stress increment before the peak stress. After reaching the elastic limit, the internal cracks are initiated and progressed with the increase of strain. In the meantime, the fibres in EGC start to bridge the cracks and restrain the crack growth. Besides, a certain amount of energy is required to de-bond the fibres from the geopolymer matrix and initiate the pull-out of fibres. After exceeding the peak stress, the cracks are further propagated and expanded, leading to visible cracks [46, 70]. Furthermore, most of the fibres in EGC undergo sliding/slippage during the pull-out process up to the final failure of tested specimens. Although a similar shape of stress-strain response can be observed for different mixtures, the resultant values of stress and strain in various stages (e.g., peak stress) were different which will be discussed further in the following sections.

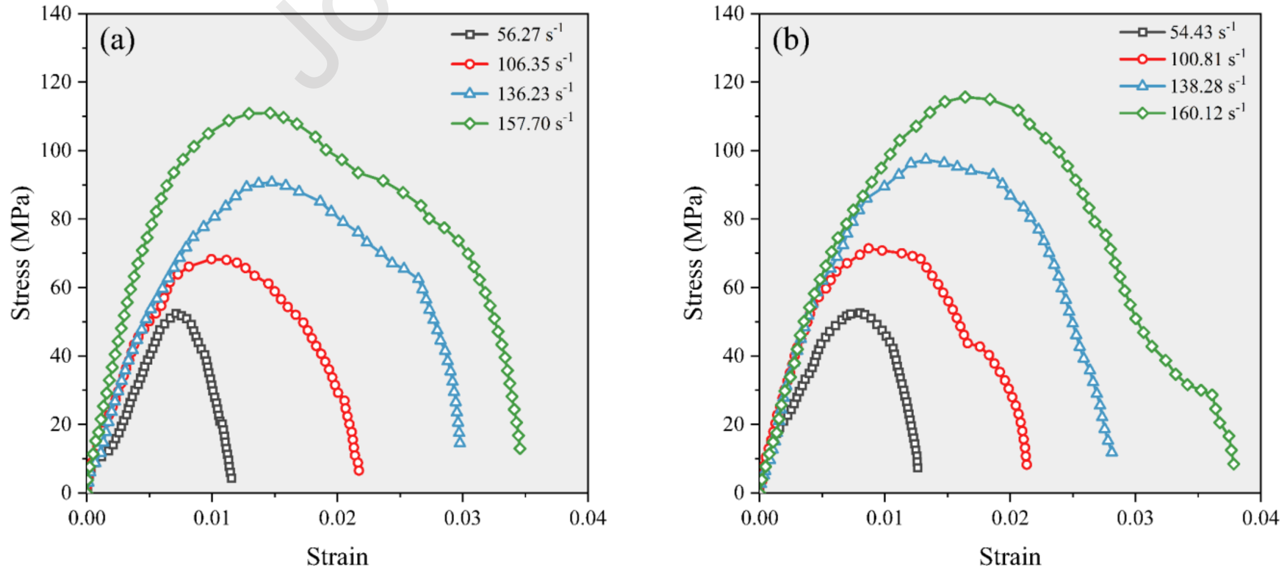

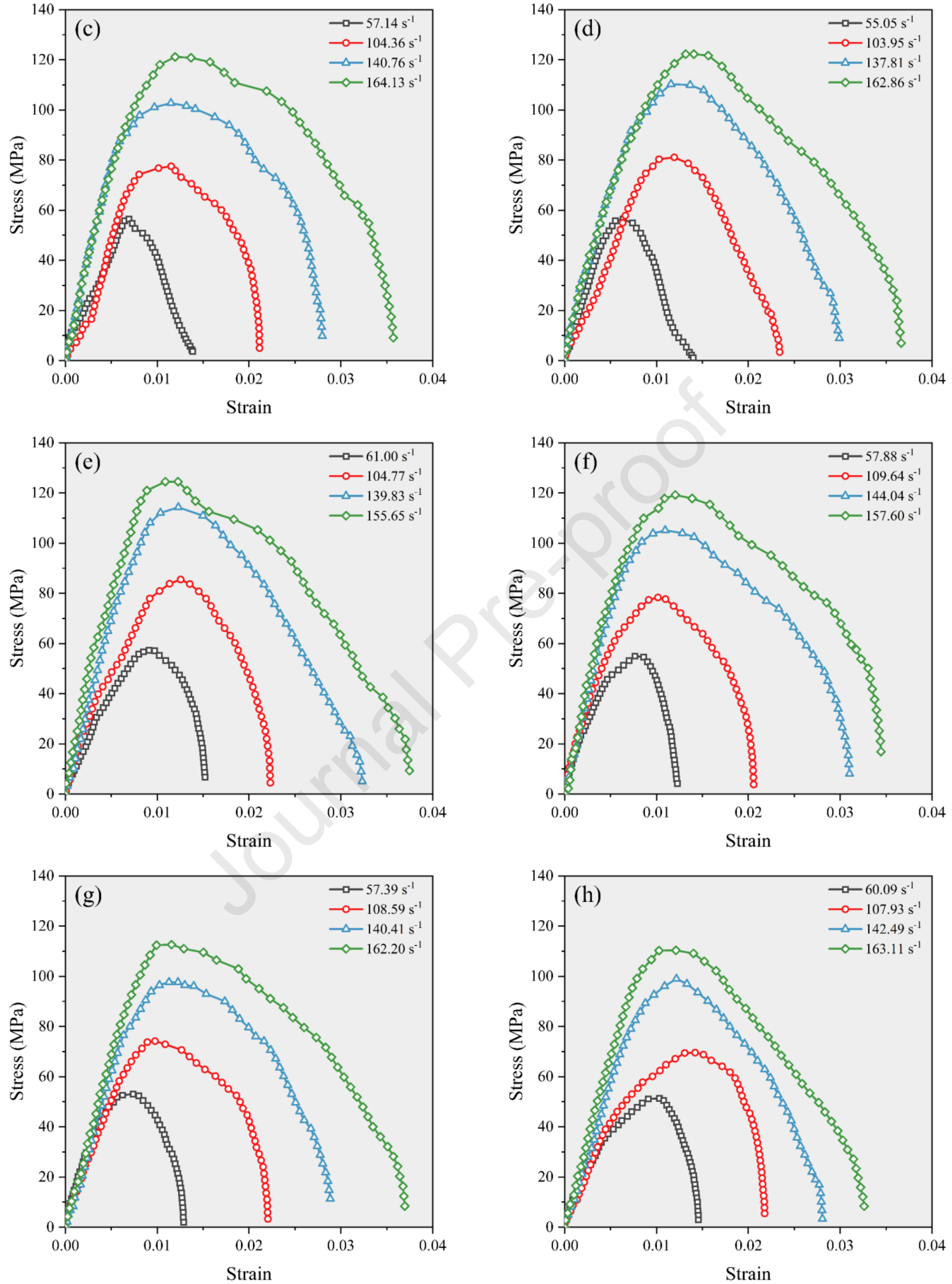

Fig. 11. Representative stress-strain curves of all mixtures: (a) P0R0; (b) P1.0R0; (c) P1.5R0; (d) P2.0R0; (e) P1.75R0.25; (f) P1.5R0.5; (g) P1.25R0.75; (h) P1.0R1.0

3.4.2. Failure pattern

Figs. 12 and 13 demonstrate the typical failure patterns of all mixtures at various strain rates, indicating that the damage degree and integrity loss of all mixtures were increased with the increasing strain rate. At a low strain rate (56.27 s^{-1}), the plain geopolymer mixture (P0R0) exhibited prominent longitudinal splitting failure with several fragments with irregular sizes (Fig. 12a). When the strain rate raised, the damage on P0R0 became more severe with more and smaller fragments. The crack velocity tended to be lower at a low strain rate, which allowed the cracks to go through the weak zones to propagate from the edge of the specimen towards its core area [46, 71]. Thus, several large fragments can be observed for the failed specimen. As the strain rate increased, the applied stress and crack velocity went up rapidly to generate more cracks to consume the energy before the cracks had sufficient time to seek the weak zone to propagate [46, 72] as crack generation requires more energy than crack propagation. Therefore, the specimen fractured into more fragments with smaller sizes at a high strain rate.

As seen in Figs. 12b-d, the incorporation of PVA fibres reduced the damage degree of specimens under various strain rates compared to P0R0 (Fig. 12a). When the strain rate was lower (54.43-104.36 s^{-1}), P1.0R0, P1.5R0 and P2.0R0 maintained the cylindrical shapes of specimens along with some visible edge cracks after the dynamic compression due to the bridging effect of fibres that can effectively prevent the matrix from breaking into fragments and improves the impact resistance. Similar findings were reported for steel and PVA fibre reinforced geopolymer composites [42, 73]. As the strain rate increased to about 140 s^{-1}, all PVA fibre reinforced EGC specimens started to disintegrate and presented fragmental failure, while fewer fragments with larger sizes can be found if the PVA fibre dosage was high (Fig. 12d). With the further increase of strain rate to about 160 s^{-1}, more fragments with irregular sizes can be observed for all PVA fibre reinforced EGC, mainly due to the less bridging fibres across the cracking interfaces induced by the increased crack size at a high strain rate [74]. More fibres were either pulled out or ruptured under high-velocity impact loads.

As displayed in Fig. 13, the hybrid fibre reinforced EGC had similar failure patterns with P2.0R0 at different strain rates. When the strain rate exceeded approximately 140 s^{-1}, replacing PVA fibres with more RTP fibres (0.75% and 1.0%) tended to be less resistant to impact with a higher integrity loss (Figs. 13c and d). Given the length difference between PVA and RTP fibres (see Table 2), RTP fibres would be more effective in bridging the initiated internal micro-cracks while when the micro-cracks grew into macro-cracks, PVA fibres started to exert the crack-arresting ability. Fewer RTP fibres can be found in bridging the crack interfaces of failed specimens as they were mostly pulled out with the crack development. Thus, when an appropriate content of PVA fibres is replaced with RTP fibres, the synergistic effects of them can lead to better impact behaviour compared to mono-PVA fibre reinforced EGC. Besides, fibre-matrix bonding and fibre orientation also play essential roles in reducing the damage degree of EGC after dynamic compression [46]. Regarding fibre orientation, inconsistent conclusions can be found in the literature revealing that better impact resistance can be achieved when fibres are distributed either parallel [75] or perpendicular [76] to the loading direction. Given the different failure patterns here, fibres aligned perpendicular to the loading direction could be more effective in bridging and restraining the longitudinal splitting cracks along the edge of the specimen and the transverse cracks around the centre surface of the specimen. The failure patterns discussed above can only be used to qualitatively assess the impact resistance of materials while the quantitative analysis will be given below.

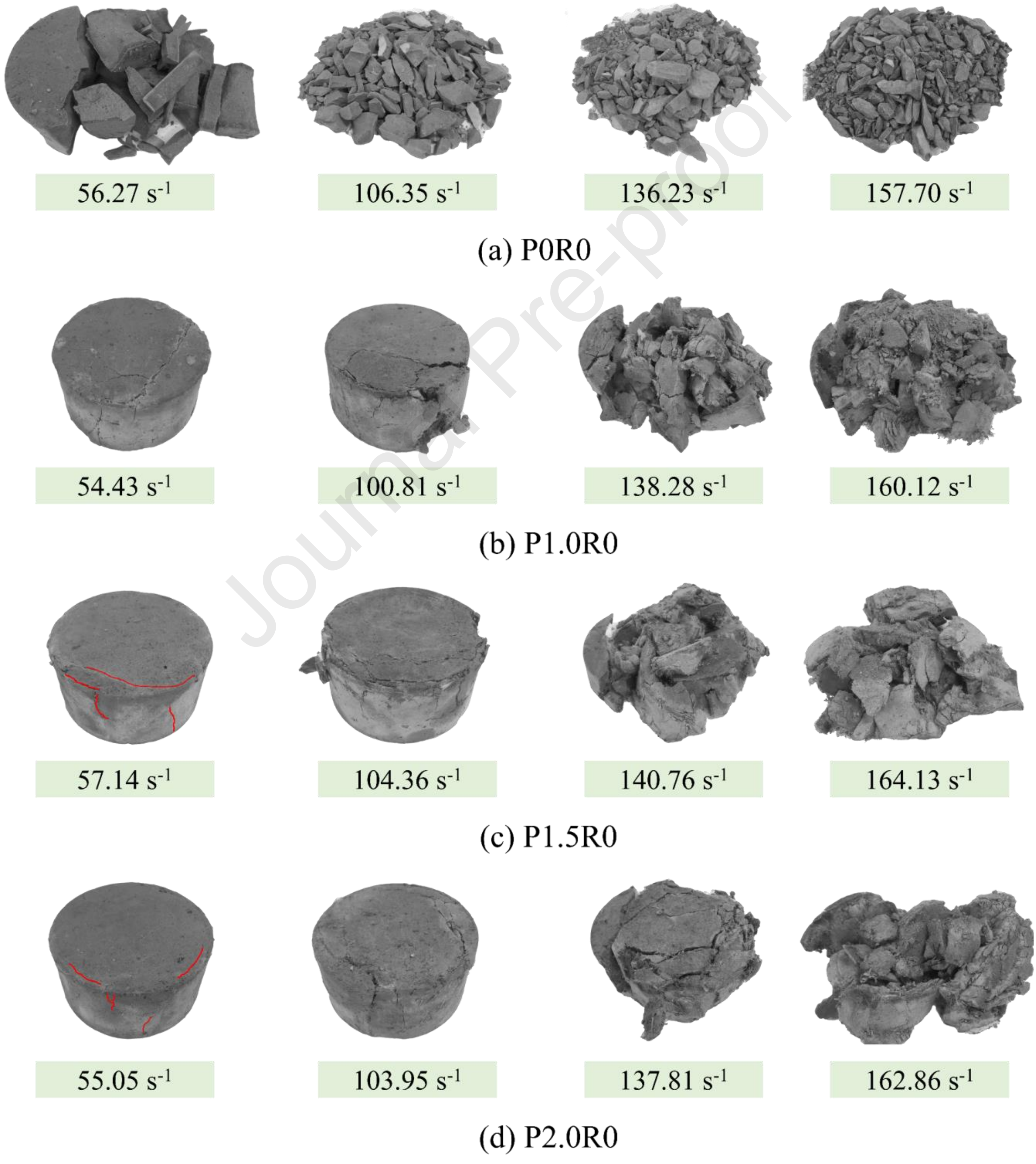

Fig. 12. Typical failure patterns of plain mixture and mono-PVA fibre reinforced EGC at different strain rates.

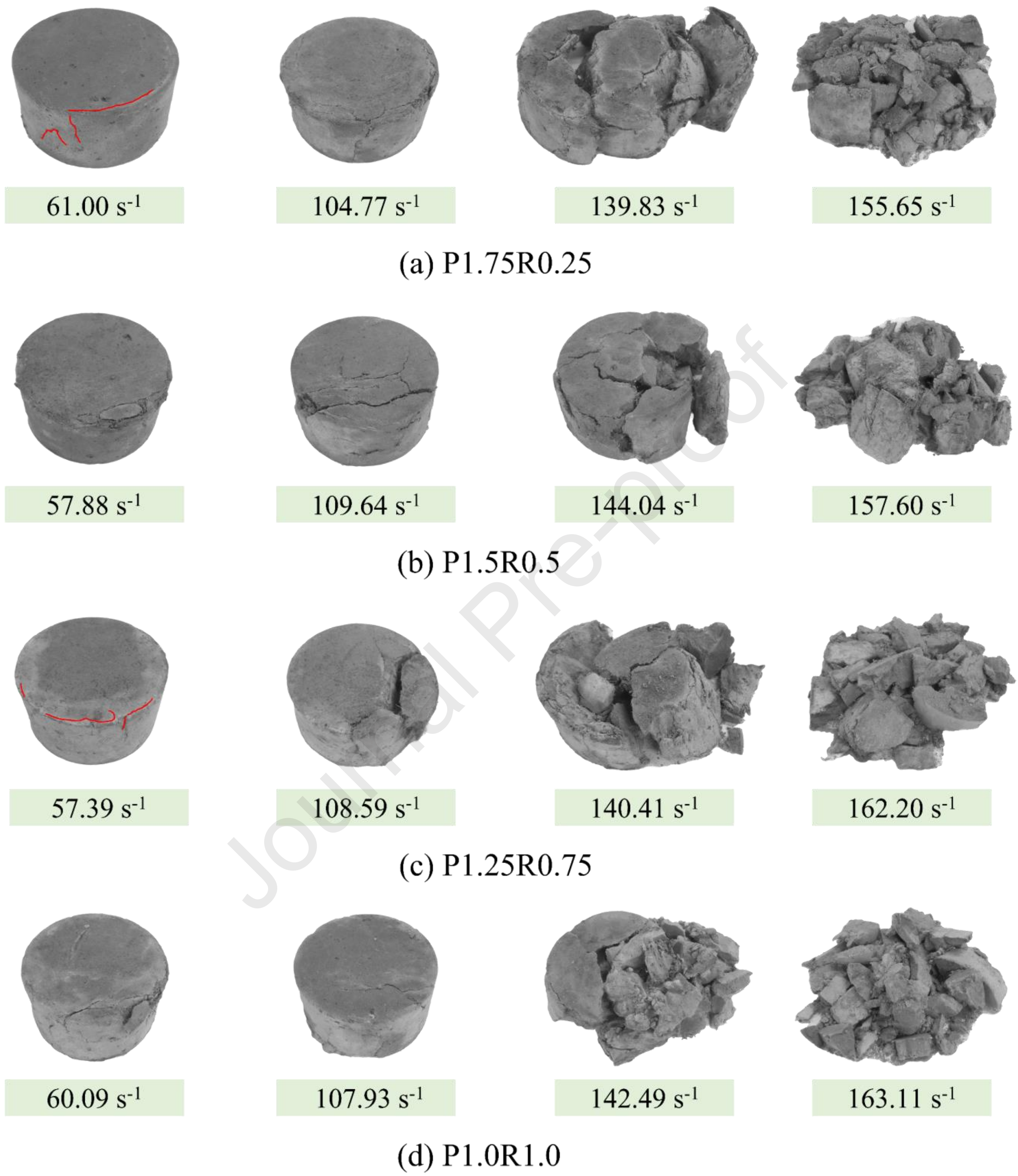

Fig. 13. Typical failure patterns of hybrid PVA and RTP fibre reinforced EGC at different strain rates.

3.4.3. Dynamic compressive strength

Fig. 14 demonstrates the dynamic compressive strength of all mixtures at different strain rates, which indicates that all mixtures exhibited a similar feature that the dynamic compressive strength was enhanced with the increase of strain rate. For instance, the dynamic compressive strength of P0R0 was increased by 30.88-115.95% when the strain rate changed from 56.27 s^{-1} to 106.35 s^{-1}, 136.23 s^{-1} and 157.7 s^{-1}, respectively, which can be ascribed to the structural effects (lateral inertia and end friction confinement), time-dependent crack propagation effect and Stefan effect induced by the viscosity of free water [77-79]. As mentioned in Section 2.4.3, some approaches have been applied to mitigate the structural effects. Besides, it was reported that a significant lateral inertia effect only appears when the strain rate is over 200 s^{-1} [80]. Thus, it can be assumed that the strength enhancement observed in this study could be mainly caused by the crack propagation effect (see Section 3.4.2) and the Stefan effect. Regarding the Stefan effect, the free water between cracks would create a viscous force to hinder the crack propagation under high-velocity impact loading (i.e., improving the strength) instead of generating a wedging effect to favour the crack propagation at a low strain rate [71, 81]. The viscous force tends to be higher at a higher crack velocity (larger strain rate) which can further enhance the dynamic compressive strength of specimens.

Unlike the quasi-static compressive strength, the addition of PVA fibres increased the dynamic compressive strength of geopolymers. For instance, as seen in Fig. 14, within the strain rate of 100.81-109.64 s^{-1}, the dynamic compressive strengths of P1.0R0, P1.5R0 and P2.0R0 were 6.98%, 12.37% and 17.22% higher than that of P0R0. The crack propagation under the quasi-static loading is similar to that under the dynamic loading at a low strain rate, where the cracks can go through the weak zones to propagate. As discussed in Sections 3.1 and 3.2, the porosity of EGC can be higher due to the additional air entrapped by PVA fibres, and thus fewer fibres can offer bridging effects under quasi-static loading as the cracks tend to propagate through the induced voids caused by the fibres [51]. As mentioned previously, the crack velocity raised with the increasing strain rate and more cracks were generated before the cracks had enough time to reach the weak zones. Meanwhile, more PVA fibres can exert their effects to bridge and restrain the induced cracks. Different from plain geopolymer, an additional amount of energy was required to pull out or rupture the fibres in EGC. Hence, the dynamic compressive strength can be improved by the bridging effect of PVA fibres under various strain rates, which is consistent with the findings reported in Refs. [71, 82] that polypropylene fibre reinforced concrete had comparable or lower quasi-static compressive strength but higher dynamic compressive strength under various strain rates (25-125 s^{-1}) as compared with plain concrete.

Besides, the fibre-matrix interface properties would also strongly affect the dynamic compressive properties of EGC. Compared to other synthetic fibres, PVA fibres possess special interface characteristics in terms of chemical bonding, frictional bonding and slip-hardening coefficient [83], which are related to the microstructure and properties of the matrix, e.g., fracture toughness [20]. To facilitate the pull-out process of PVA fibre, the applied stress should first overcome the chemical bonding to de-bond the fibre from the matrix followed by the slippage/sliding of the fibre governed by the frictional bonding and slip-hardening coefficient [1]. Moderate frictional bonding and slip-hardening coefficient are desirable to induce fibre pull-out instead of fibre rupture. It was found that the interface properties between PVA fibre and matrix especially frictional bonding can be improved with the increasing strain rate [84, 85]. Besides, the mechanical properties of PVA fibres (e.g., tensile strength) can be enhanced with the increase of strain rate [86]. These combined effects can cause an increased number of pulled out PVA fibres as the strain rate rises, leading to an increase in dynamic compressive strength of EGC. This finding can be detected in Fig. 15a that more PVA fibres were pulled out instead of ruptured under dynamic loading, which is in good agreement with a previous study [31] demonstrating that the failure mode of PVA fibre in EGC changed from fibre rupture under quasi-static loading to fibre pull-out under dynamic loading. Hence, the strength improvement of PVA fibre reinforced EGC over P0R0 was found to rise with the increase of strain rate up to about 140 s^{-1}. For instance, the dynamic compressive strengths of P2.0R0 at the strain rates of 55.05 s^{-1}, 103.95 s^{-1} and 137.81 s^{-1} were found to be about 6.80%, 17.22% and 18.88% higher than that of P0R0 under similar strain rates (Fig. 14). However, as the strain rate went up to around 160 s^{-1}, the strength improvement ratio of PVA fibre reinforced EGC over P0R0 declined. For instance, the dynamic compressive strength of P2.0R0 was only 9.13% higher than that of P0R0, which can be ascribed to the increased crack width and superior fibre-matrix interface properties. Due to the excellent interface properties, the probability of PVA fibre rupture tended to be higher, which would reduce the fibre bridging efficiency. Many ruptured PVA fibres can be observed at the strain rate of around 160 s^{-1} (Fig. 15b). Overall, all PVA fibre reinforced EGC exhibited a higher dynamic compressive strength compared to plain geopolymer mixture under different strain rates where P2.0R0 indicated the best performance.

As illustrated in Fig. 14, partial replacement of PVA fibres with RTP fibres can result in a slightly higher or comparable dynamic compressive strength compared to EGC containing 2.0% PVA fibre. For instance, the dynamic compressive strengths of P1.75R0.25 at strain rates of 61 s^{-1}, 104.77 s^{-1}, 139.83 s^{-1} and 155.65 s^{-1} were approximately 3.57%, 5.34%, 2.34% and 0.62%, respectively greater than that of P2.0R0 under similar strain rates. Besides, P1.5R0.5 showed a comparable dynamic compressive strength to P2.0R0 with a difference of no more than 3.42%. Like PVA fibre, the mechanical and interface properties of RTP fibre could be improved with the increase of strain rate. The use of hybrid PVA fibre and a small amount of RTP fibre in EGC can lead to desirable fibre orientation and the synergistic effect of hybrid fibres at different scales can be effectively employed to bridge and restrain the induced cracks under dynamic loadings. As shown in Fig. 15c, RTP fibres were mostly pulled out due to their shorter lengths while longer PVA fibres can better provide the crack-resistance action as the cracks developed. Besides, the fibre spacing of RTP fibres in EGC tended to be smaller compared to that of PVA fibres due to the shorter length under a given volume of fibre reinforcement [37]. As such, more RTP fibres can contribute to the bridging effect around a single micro-crack to prevent it from further growth and coalescence into a macro-crack and thus improve the impact resistance of EGC. EGC with RTP fibre could contain more free water than PVA fibre reinforced EGC due to the release of temporarily blocked water content at the surface of RTP fibre [17, 87], which would lead to an improvement in dynamic compressive strength due to the Stefan effect [81]. The interface properties of RTP fibre at a higher strain rate were still significantly lower as compared with PVA fibre due to the inherent hydrophobic surface feature of RTP fibre, as displayed in Fig. 15a and c that more matrix fragments were adhered on the PVA fibre surfaces, while RTP fibres had smooth surfaces with less attached matrix fragments. Thus, with the substitution of RTP fibre (0.75-1.0%) for PVA fibre in EGC, a 4.21-13.17% reduction in dynamic compressive strength can be observed in comparison with P2.0R0. To conclude, most hybrid fibre reinforced EGC mixtures can outperform the plain geopolymer mixture in terms of dynamic compressive strength and adding a small amount of RTP fibre into EGC is beneficial to the dynamic compressive strength of EGC mainly because of the synergistic effect of hybrid fibres in arresting and controlling the cracks.

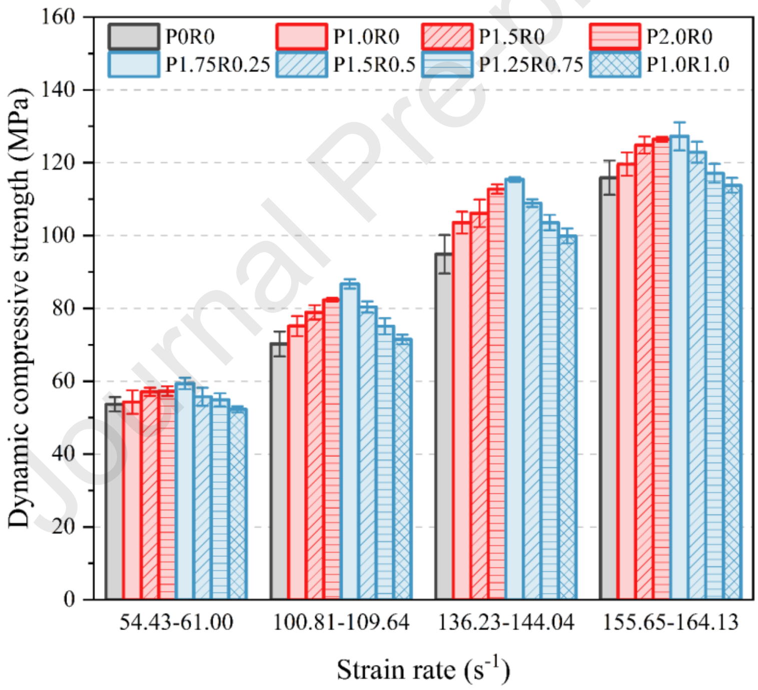

Fig. 14. Effects of strain rate and fibre on dynamic compressive strength of geopolymer mixtures.

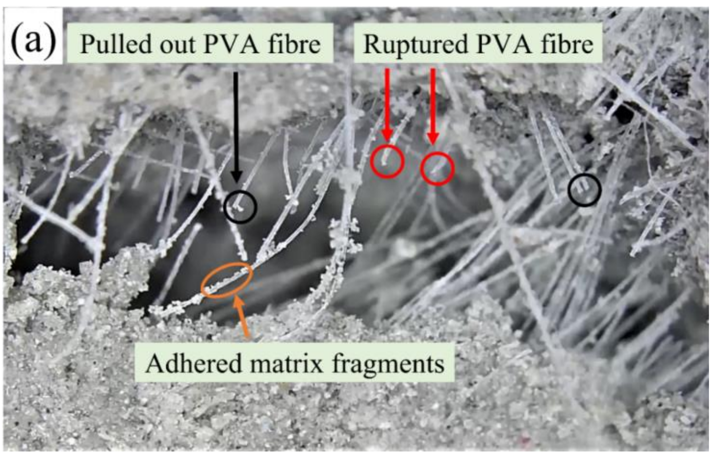

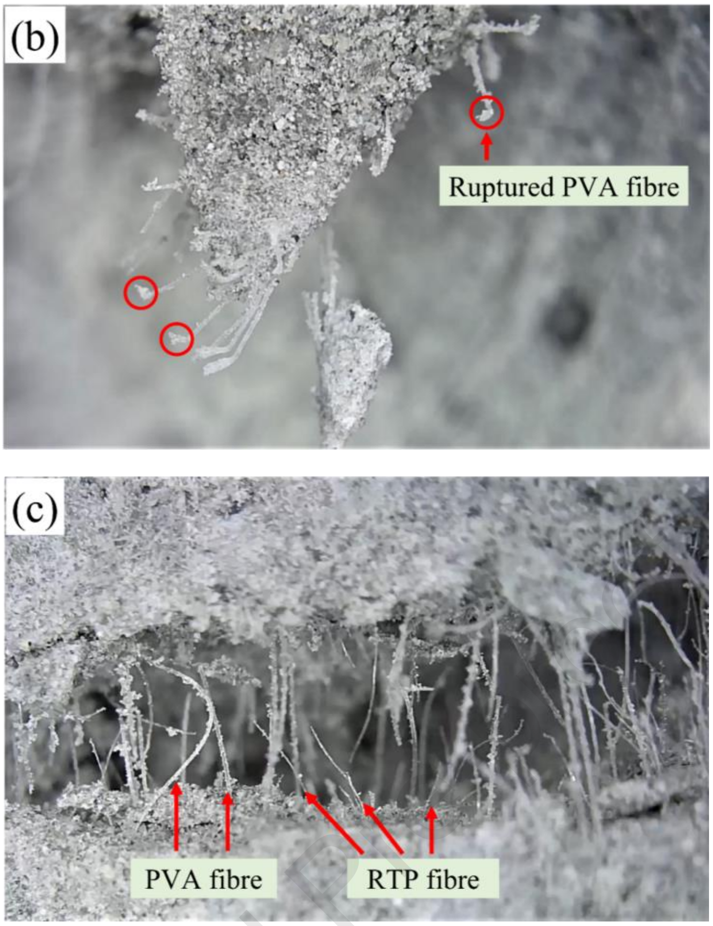

Fig. 15. Fibre conditions at the cracking interfaces after dynamic compression.

3.4.4. Dynamic increase factor

DIF is defined as the ratio of dynamic compressive strength to quasi-static compressive strength. Acquiring a reliable relationship between DIF and strain rate can better characterise the strain rate sensitivity of materials under high-velocity impact loads and can offer more insights for future structural design and numerical study [58]. To this end, the experimental scatters of DIF and strain rate were used to develop the DIF equations for all mixtures, the results of which are illustrated in Fig. 16 and Table 4. In this study, the transition strain rate was considered, which divided the proposed DIF equations into two parts [42, 68, 88]. It was reported that the strength improvement of materials as the change of strain rate is not pronounced below the transition strain rate while over which, the strength would go up considerably [88]. As seen in Fig. 16, the DIF of all mixtures was improved significantly with the increasing strain rate after exceeding the transition strain rate ranging from 56.15 s^{-1} to 67.51 s^{-1}, which can be due to the reasons explained for dynamic compressive strength (see Section 3.4.3). When the fibre content changed, the variation of transition strain rate was not consistent. Khan et al. [42] found that the transition strain rate of fibre reinforced geopolymer composites was 66 s^{-1} which was higher than that of plain geopolymers (30 s^{-1}). This can be ascribed to the reduced lateral deformation as a result of the fibre bridging behaviour, leading to a higher triggering rate to change the properties of composites [89]. Besides, the transition strain rate can be affected by the combined effect of fibre content, fibre shape and matrix strength [88]. As shown in Table 4, the developed first-part DIF equations of P0R0, P1.0R0 and P1.0R1.0 had lower reliability considering their R^2 values. By contrast, other proposed first-part DIF equations seemed reliable due to their higher R^2 values (mostly larger than 0.9). In general, to further increase the reliability of the first-part DIF equations and better understand the transition strain rate, more DIF data at the low strain rates especially quasi-static (10^{-4}-10^{-3} s^{-1}) and intermediate strain rates (10^{-3}-1 s^{-1}) are required.

Regardless of fibre type and content, the presence of fibres enhanced the strain rate sensitivity of geopolymers given that the second-part DIF equations of EGC mixtures had higher gradients ranging from 2.559 to 3.178 compared to P0R0 (Fig. 16), which can be ascribed to the additional resistance provided by the fibres under dynamic loadings. This is in good agreement with previous studies on geopolymer composites [42, 73]. For instance, it was found that the DIF of geopolymer composites containing 1.2% PVA fibre was increased by 3.56-4.25 times as compared with plain geopolymers under similar impact velocities [73]. Similar to dynamic compressive strength, the strain rate sensitivity of EGC was improved with the increase of PVA content while the strain rate sensitivity reduced when the RTP fibre content was over 0.25%. As observed in Fig. 16, P1.75R0.25 exhibited the highest strain rate sensitivity among all mixtures and the strain rate sensitivity of P1.5R0.5 was comparable with that of P2.0R0. The mechanisms behind these were similar to those provided in Section 3.4.3. This further suggests that replacing PVA fibres with a small amount of RTP fibres can lead to better dynamic compressive properties. The proposed second-part DIF equations of all mixtures shown in Table 4 had high reliability as most of the R^2 values were greater than 0.9.

Fig. 17 shows the DIF results obtained from this study in comparison with the predictions using the existing DIF models [63, 90] and the results obtained from literature on geopolymer composites [42, 73]. The DIF models proposed by the FIB model code [90] and CEB-FIP model code [63] have high accuracy and reliability for normal-strength concrete with a transition rate of 30 s^{-1}:

$$DIF_{FIB} = (\frac{\dot{\varepsilon}}{\dot{\varepsilon}_1})^{0.014} \ for\ \dot{\varepsilon} \le 30\ s^{-1} \tag{6}$$

$$DIF_{FIB} = 0.012(\frac{\dot{\varepsilon}}{\dot{\varepsilon}_1})^{\frac{1}{3}} \ for\ \dot{\varepsilon} > 30\ s^{-1} \tag{7}$$

$$DIF_{CEB-FIP} = (\frac{\dot{\varepsilon}}{\dot{\varepsilon}_1})^{1.026\alpha} \ for\ \dot{\varepsilon} \le 30\ s^{-1} \tag{8}$$

$$DIF_{CEB-FIP} = \gamma(\frac{\dot{\varepsilon}}{\dot{\varepsilon}_1})^{\frac{1}{3}} \ for\ \dot{\varepsilon} > 30\ s^{-1} \tag{9}$$

where $\dot{\varepsilon}_1$ is equal to 0.00003 s^{-1}, α is $(5 + 9\frac{f_c}{f_{c1}})^{-1}$, γ is $10^{(6.156\alpha - 2)}$, f_c is the quasi-static compressive strength, and f_{c1} = 10 MPa.

The above equations indicate that the FIB model code ignores the quasi-static compressive strength while the CEB-FIP model code has taken it into account. In this study, 50 MPa was selected as the input of the CEB-FIP model. As seen in Fig. 17, the predicted results of DIF using the above models were higher than the results obtained from this study when the strain rate was less than 100 s^{-1}, which can be attributed to the lower transition strain rates of the models proposed by FIB and CEB-FIP. The differences in between were reduced with the increasing strain rate. It is worth noting that when the strain rate reached about 160 s^{-1}, the DIF of the plain geopolymer mixture was comparable to that predicted by the models while all EGC exhibited higher DIF values. On the other hand, Fig, 17 reveals that at a higher strain rate (e.g., 140 s^{-1}), the mixtures containing solely synthetic fibres possessed higher DIF values than the mixtures containing steel fibres, implying a lower strain rate sensitivity for steel fibre reinforced composites. Similar results have been reported in Refs. [70, 78], which can be ascribed to the superior internal quality of steel fibre reinforced composites with lower porosity and fewer internal flaws as concrete with poorer quality can lead to higher DIF under dynamic loadings [70, 88, 91]. Besides, the lower strain rate sensitivity of steel itself compared to the matrix may contribute to the smaller DIF values [92].

Table 4 Summary of fitted logarithm curves for all mixtures.

Mixture	Fitted equation	Strain rate range	R^2
P0R0	$DIF = 0.00507Log\dot{\varepsilon} + 1.0209$	$10^{-5}\, s^{-1} \le \dot{\varepsilon} \le 62.04\, s^{-1}$	0.1524
	$DIF = 2.370Log\dot{\varepsilon} - 3.1972$	$\dot{\varepsilon} > 62.04\, s^{-1}$	0.8064
P1.0R0	$DIF = 0.00805Log\dot{\varepsilon} + 1.0326$	$10^{-5}\, s^{-1} \le \dot{\varepsilon} \le 59.07\, s^{-1}$	0.1482
	$DIF = 2.559Log\dot{\varepsilon} - 3.4702$	$\dot{\varepsilon} > 59.07\, s^{-1}$	0.9055
P1.5R0	$DIF = 0.0258Log\dot{\varepsilon} + 1.050$	$10^{-5}\, s^{-1} \le \dot{\varepsilon} \le 64.15\, s^{-1}$	0.9059
	$DIF = 2.792Log\dot{\varepsilon} - 3.8306$	$\dot{\varepsilon} > 64.15\, s^{-1}$	0.9062
P2.0R0	$DIF = 0.0318Log\dot{\varepsilon} + 1.1295$	$10^{-5}\, s^{-1} \le \dot{\varepsilon} \le 56.15\, s^{-1}$	0.9092
	$DIF = 2.930Log\dot{\varepsilon} - 3.9920$	$\dot{\varepsilon} > 56.15\, s^{-1}$	0.9330
P1.75R0.25	$DIF = 0.0343Log\dot{\varepsilon} + 1.1401$	$10^{-5}\, s^{-1} \le \dot{\varepsilon} \le 67.51\, s^{-1}$	0.9059
	$DIF = 3.178Log\dot{\varepsilon} - 4.4951$	$\dot{\varepsilon} > 67.51\, s^{-1}$	0.9437
P1.5R0.5	$DIF = 0.0270Log\dot{\varepsilon} + 1.1103$	$10^{-5}\, s^{-1} \le \dot{\varepsilon} \le 62.39\, s^{-1}$	0.8238
	$DIF = 2.987Log\dot{\varepsilon} - 4.1789$	$\dot{\varepsilon} > 62.39\, s^{-1}$	0.9022
P1.25R0.75	$DIF = 0.0312Log\dot{\varepsilon} + 1.1274$	$10^{-5}\, s^{-1} \le \dot{\varepsilon} \le 58.79\, s^{-1}$	0.9341
	$DIF = 2.871Log\dot{\varepsilon} - 3.9633$	$\dot{\varepsilon} > 58.79\, s^{-1}$	0.9031
P1.0R1.0	$DIF = 0.0239Log\dot{\varepsilon} + 1.0973$	$10^{-5}\, s^{-1} \le \dot{\varepsilon} \le 61.91\, s^{-1}$	0.6342
	$DIF = 2.994Log\dot{\varepsilon} - 4.2823$	$\dot{\varepsilon} > 61.91\, s^{-1}$	0.9114

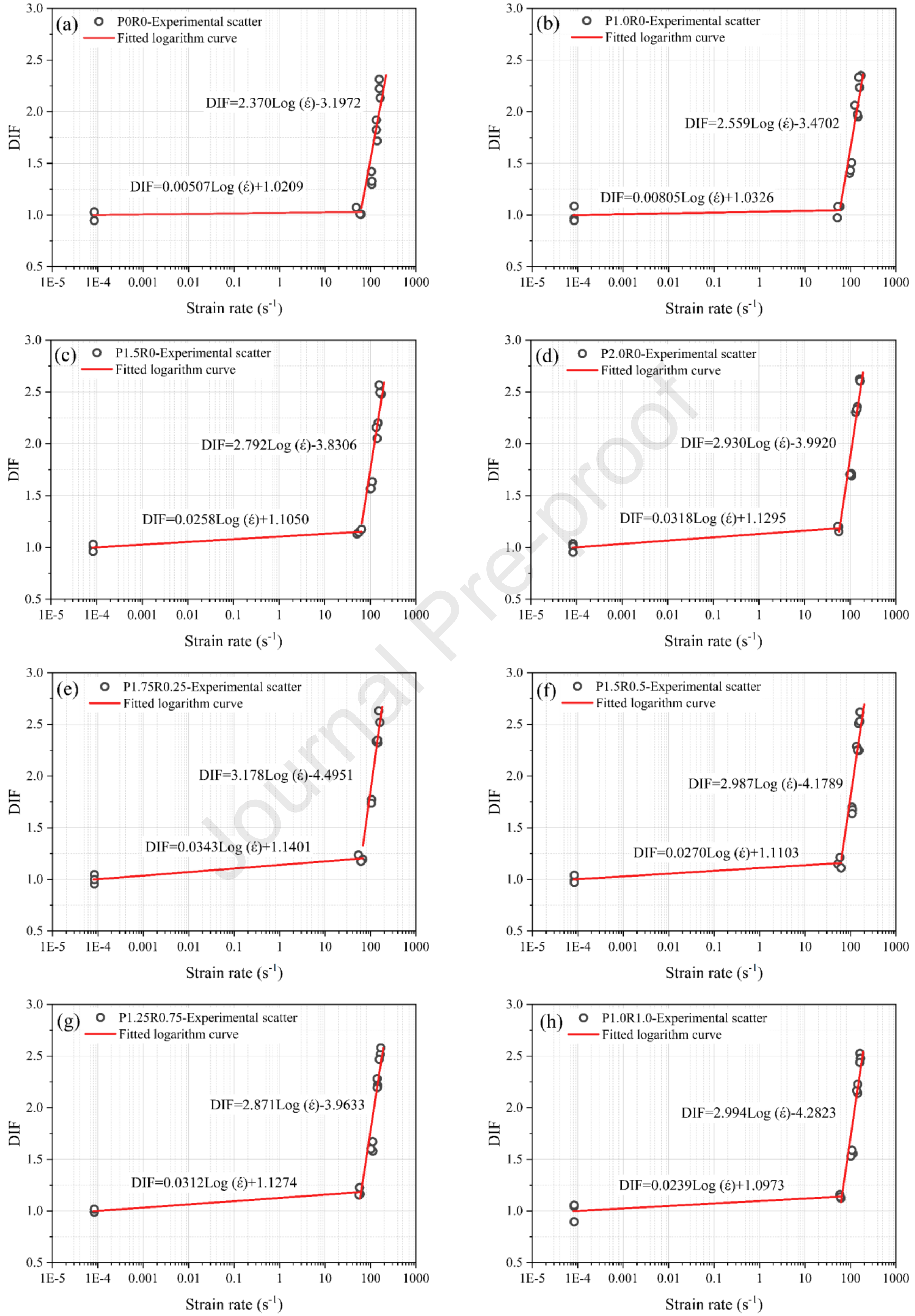

Fig. 16. Relationship between dynamic increase factor (DIF) and strain rate for all mixtures.

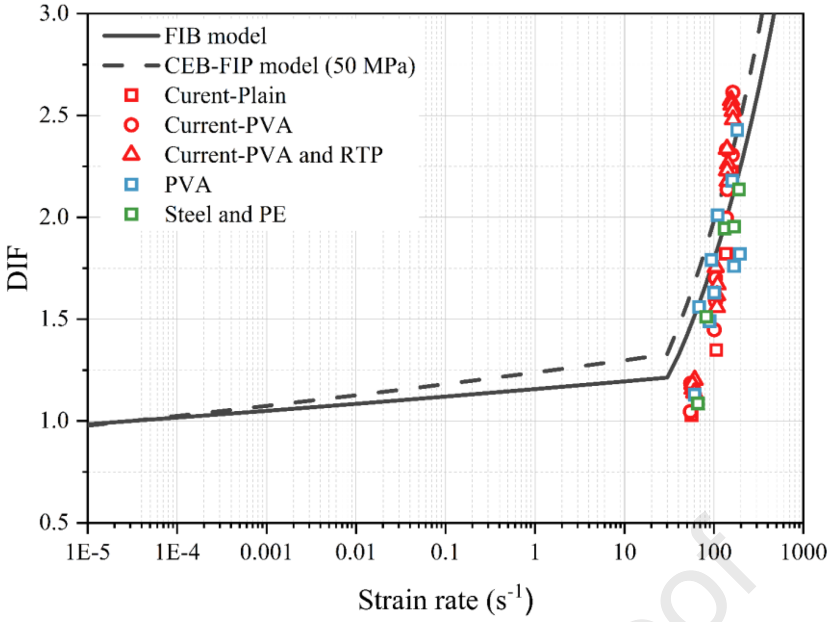

Fig. 17. Comparison of DIF obtained from the current study with the predictions and literature data [42, 63, 73, 90].

3.4.5. Energy absorption capacity

The energy absorption capacity of all mixtures under dynamic loadings can be represented by the area under the entire stress-strain curve shown in Fig. 11, the results of which are presented in Fig. 18 considering the effects of strain rate and fibre. As discussed in Section 3.4.1, the energy absorption capacity of the mixture is significantly increased after the elastic stage as the generation and propagation of cracks as well as the fibre pull-out (for EGC only) mainly appear after reaching the elastic limit. Consistent with dynamic compressive strength and DIF, the energy absorption capacity of all mixtures was considerably enhanced with the increasing strain rate (Fig. 18). For instance, the energy absorption capacity of P2.0R0 was increased by 157.43%, 387.64% and 551.90% when the strain rate raised from 55.05 s^{-1} to 103.95 s^{-1}, 137.81 s^{-1} and 162.86 s^{-1}, respectively. This can be partially due to the improved dynamic compressive strength as a result of the combined action of time-dependent crack propagation and Stefan effect (Section 3.4.3). It should be noted that the energy absorption considered in this study is not only affected by strength but also strain (deformation). As seen in Fig. 11, the strain at the peak stress of all mixtures known as peak strain was mostly improved with the increase of strain rate as a result of the enhanced cumulative strain at the appearance of more cracks [66], which contributes to the overall improvement of energy absorption capacity.

The SEM images of PVA and RTP fibres in EGC are presented in Figs. 19 and 20, respectively, which can provide more details about the fibre surface condition after dynamic loadings and help interpret the test results. As pointed out above, the presence of fibres was beneficial to the energy absorption capacity of geopolymers under various strain rates. Within the strain rate range of 54.43-109.64 s^{-1}, increasing the PVA fibre content from 1.0% to 2.0% did not obviously improve the energy absorption capacity, which can be ascribed to the insignificant improvement in dynamic compressive strength caused by the increased PVA fibre dosage under these strain rates (Fig. 14). As mentioned earlier, the increase of strain rate can improve the mechanical and interface properties of PVA fibres, which facilitates the fibre pull-out rather than fibre rupture. Thus, within the strain rate range of 136.23-144.04 s^{-1}, the energy absorption capacity of P2.0R0 was the highest among all mono-PVA fibre reinforced EGC, which was approximately 11.06% and 2.87% higher than that of P1.0R0 and P1.5R0, respectively. More pulled out PVA fibres can be observed along with some pronounced traces after PVA fibre pull-out (Figs. 19a and b). However, with the further increase of strain rate, the energy absorption capacity of EGC was not improved as the PVA dosage increased from 1.5% to 2.0% (Fig. 18), which can be associated with the reduced fibre efficiency (see Section 3.4.3). As seen in Fig. 19d, due to the considerably high interface properties of PVA fibre, it ruptured when the applied stress exceeded its tensile strength during the pull-out process, which can weaken the energy absorption capacity as fibre pull-out can absorb more energy than fibre rupture [93].

As illustrated in Fig. 18, replacing PVA fibre with a certain amount of RTP fibre (0.25-0.5%) led to a better or comparable energy absorption capacity as compared with P2.0R0. For instance, the energy absorption capacity of P1.75R0.25 was about 5.12-30.65% higher than that of P2.0R0 under various strain rates. This can be primarily attributed to the enhanced dynamic compressive strength caused by the synergistic effect between PVA and RTP fibres in controlling the cracks, smaller fibre spacing of RTP fibres and possibly increased free water content (see Section 3.4.3). Additionally, the flexible feature of RTP fibre can enhance its efficiency in bridging and restraining cracks (Fig. 20a). Although the increase of strain rate may improve the mechanical and interface properties of RTP fibre, it still exhibited pull-out behaviour due to the intrinsic hydrophobic feature, which can be identified in Fig. 20. As seen in Figs. 19c and 20b, the RTP fibre's surface had fewer attached matrix fragments as compared with PVA fibre. Under compressive loading with a high strain rate, the pull-out behaviour of RTP fibre can compensate for the loss of energy absorption capacity induced by the ruptured PVA fibre. Thus, substituting a small amount of RTP fibre for PVA fibre in EGC can help enhance the energy absorption capacity of EGC. Lu et al. [94] found a similar phenomenon that replacing PVA fibres with recycled polyethylene terephthalate fibres led to a higher energy absorption capacity in comparison with composites containing 2.0% PVA fibre because of the larger number of pulled out polyethylene terephthalate fibres under impact loading. On the other hand, due to the lower dynamic compressive strength, P1.25R0.75 and P1.0R1.0 exhibited poorer energy absorption capacity in comparison with P2.0R0, as shown in Fig. 18. Within the strain rate range of 136.23-164.13 s^{-1}, the energy absorption capacities of P1.25R0.75 and P1.0R1.0 were found to be even smaller than that of P0R0 due to the smaller peak strain values of them compared to P0R0 as their dynamic compressive strengths were comparable within the aforementioned strain rate range (Fig.

14). It was observed that the incorporation of fibres does not vary the peak strain considerably [46, 70, 74], while the peak strain is more relevant to the strain rate. Moreover, due to the incomplete fracture of some EGC mixtures, the evaluated energy absorption capacity may be slightly underestimated compared to P0R0 [42]. Overall, P1.75R0.25 and P1.5R0.5 can outperform P0R0 in terms of energy absorption capacity.

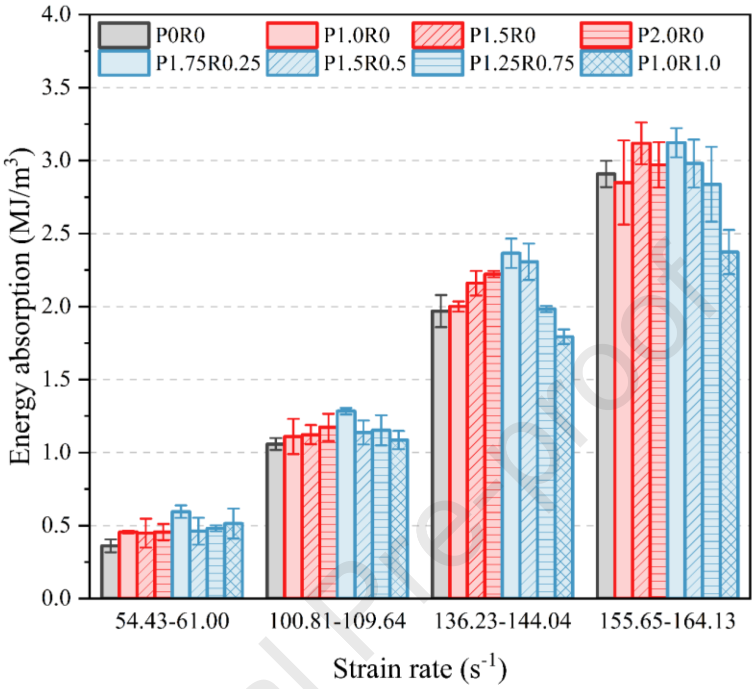

Fig. 18. Effects of strain rate and fibre on energy absorption capacity of geopolymer mixtures.

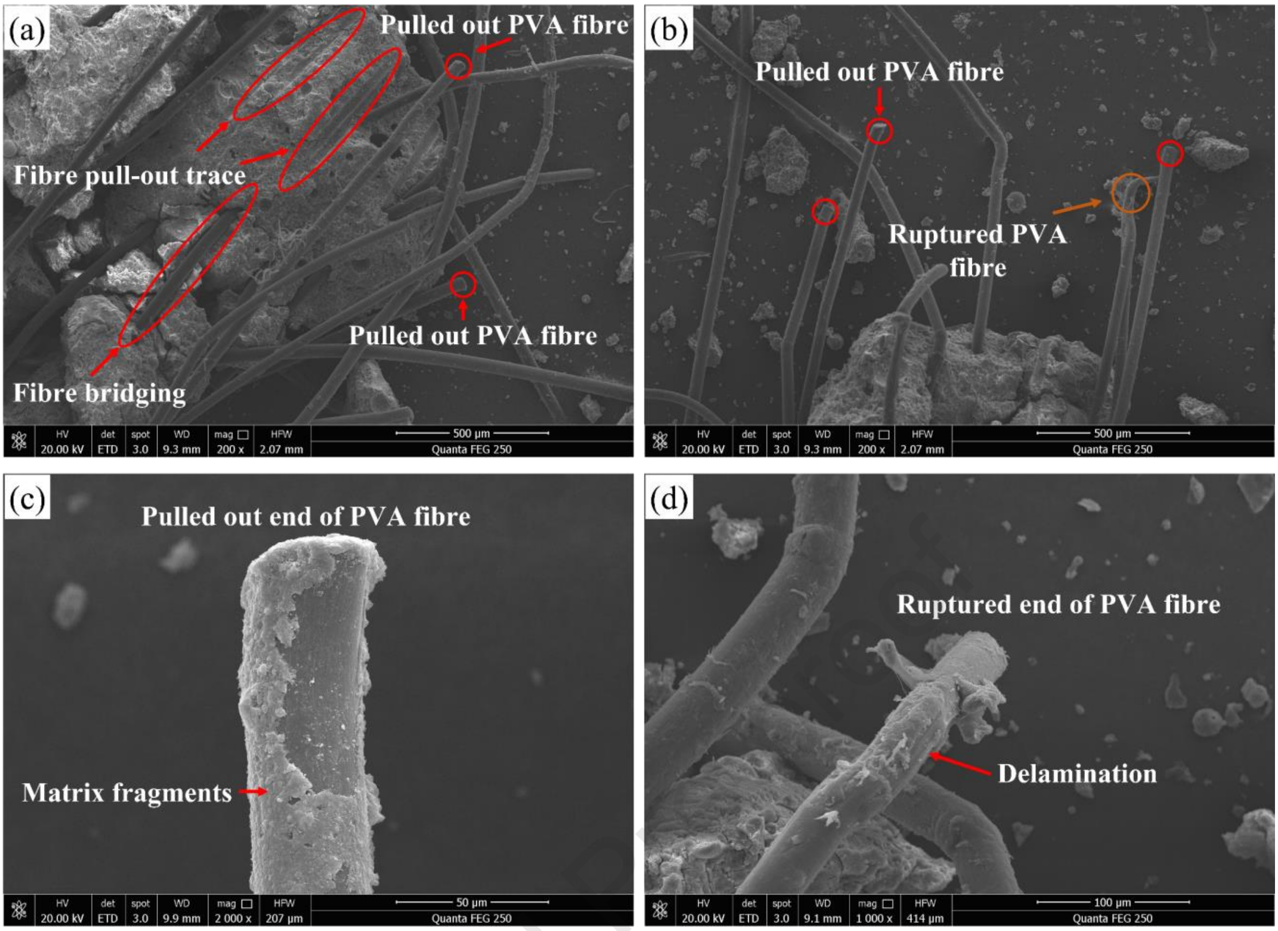

Fig. 19. SEM images of fibre morphology in PVA fibre reinforced EGC after dynamic loading.

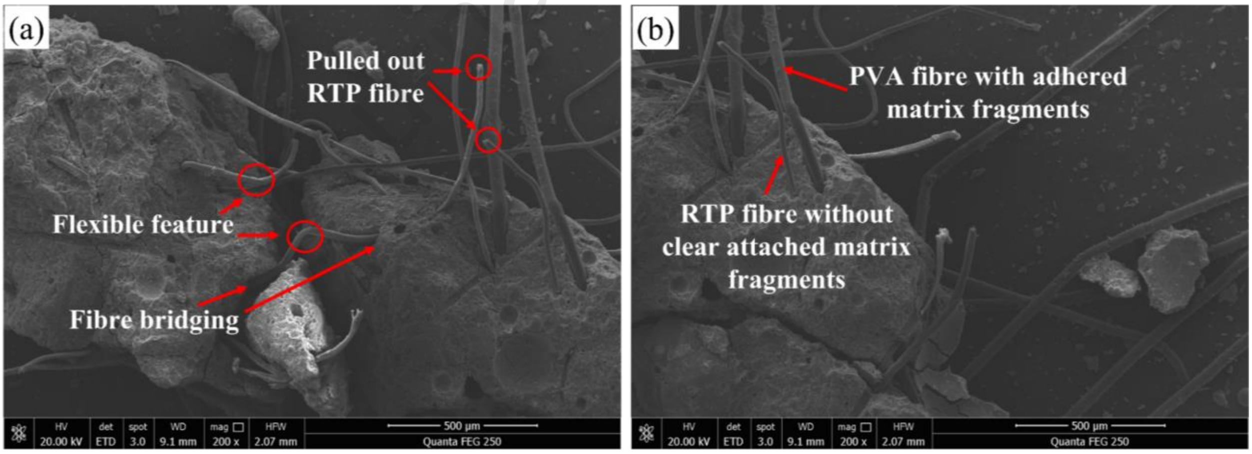

Fig. 20. SEM images of fibre morphology in hybrid fibre reinforced EGC after dynamic loading.

4. Conclusions

In this study, the effects of polyvinyl alcohol (PVA) fibre content (1.0%, 1.5% and 2.0%) and recycled tyre polymer (RTP) fibre dosage (0.25%, 0.5%, 0.75% and 1.0%) on the flowability and quasi-static compressive properties of fly ash-slag based engineered geopolymer composites (EGC) cured at ambient temperature as well as their dynamic compressive behaviour under various strain rates of 54.43-164.13 s^{-1} were investigated. Based on the experimental results obtained, the main conclusions can be drawn as follows:

- The flowability, quasi-static compressive strength and elastic modulus of EGC reduced with the increase of PVA fibre dosage while replacing PVA fibre with 0.25% RTP fibre can compensate for such loss, leading to a 2.14-25.56% improvement compared to EGC with 2.0% PVA fibre.
- The dynamic compressive behaviour including dynamic compressive strength, dynamic increase factor (DIF), failure degree and energy absorption capacity of all mixtures was sensitive to strain rate. The strain rate dependency can be well described using the proposed DIF equations with R^2 values of mostly greater than 0.9 for the considered strain rates ranging from 10^{-5} s^{-1} to 10^{3} s^{-1}.
- The incorporation of either PVA or RTP fibres can mostly improve the dynamic compressive strength, DIF, and energy absorption capacity and can all reduce the post-test damage degree of geopolymers mainly due to the additional resistance induced by the fibre bridging effect. Utilising a small amount of RTP fibre (e.g., 0.25%) to replace PVA fibre in EGC can lead to a better dynamic compressive strength, DIF and energy absorption capacity as compared with mono-PVA fibre reinforced EGC.
- SEM images indicate that more pulled out PVA fibres can be identified under dynamic loading, which was favourable for enhancing the dynamic compressive properties, especially energy absorption capacity. However, the possibility of PVA fibre rupture increased at the strain rate of 155.65-164.13 s^{-1}, which can weaken the energy absorption capacity. RTP fibres still exhibited pull-out behaviour under dynamic loadings, leading to an enhanced energy absorption capacity of EGC containing RTP fibres at various strain rates.
- EGC containing 1.75% PVA fibre and 0.25% RTP fibre can be regarded as the optimal mixture considering its highest dynamic compressive properties at various strain rates among all studied mixtures. Besides, it had adequate workability and quasi-static mechanical properties especially exhibiting the robust tensile strain-hardening behaviour as well as lower material cost and higher sustainability.

Acknowledgements

The authors gratefully acknowledge the financial support from the Engineering and Physical Sciences Research Council (EPSRC) under Grant No. EP/R041504/1 and the Royal Society under Award No. IEC\NSFC\191417. The financial support provided by University College London (UCL) and China Scholarship Council (CSC) to the first author is gratefully acknowledged.

References

[1] V.C. Li, Engineered Cementitious Composites (ECC): Bendable Concrete for Sustainable and Resilient Infrastructure, Springer 2019.

[2] Z. Zhang, F. Yang, J.-C. Liu, S. Wang, Eco-friendly high strength, high ductility engineered cementitious composites (ECC) with substitution of fly ash by rice husk ash, Cement and Concrete Research 137 (2020) 106200.

[3] T. Luukkonen, Z. Abdollahnejad, J. Yliniemi, P. Kinnunen, M. Illikainen, One-part alkali-activated materials: A review, Cement and Concrete Research 103 (2018) 21-34.

[4] M. Ohno, V.C. Li, An integrated design method of Engineered Geopolymer Composite, Cement and Concrete Composites 88 (2018) 73-85.

[5] M. Farooq, A. Bhutta, N. Banthia, Tensile performance of eco-friendly ductile geopolymer composites (EDGC) incorporating different micro-fibers, Cement and Concrete Composites 103 (2019) 183-192.

[6] B. Nematollahi, J. Sanjayan, F.U.A. Shaikh, Comparative deflection hardening behavior of short fiber reinforced geopolymer composites, Construction and Building Materials 70 (2014) 54-64.

[7] H.H. Nguyễn, Q.-H. Lương, J.-I. Choi, R. Ranade, V.C. Li, B.Y. Lee, Ultra-ductile behavior of fly ash-based engineered geopolymer composites with a tensile strain capacity up to 13.7%, Cement and Concrete Composites 122 (2021) 104133.

[8] B.Y. Lee, C.-G. Cho, H.-J. Lim, J.-K. Song, K.-H. Yang, V.C. Li, Strain hardening fiber reinforced alkali-activated mortar – A feasibility study, Construction and Building Materials 37 (2012) 15-20.

[9] S.-J. Choi, J.-I. Choi, J.-K. Song, B.Y. Lee, Rheological and mechanical properties of fiber-reinforced alkali-activated composite, Construction and Building Materials 96 (2015) 112-118.

[10] J.-I. Choi, H.H. Nguyễn, S.L. Cha, M. Li, B.Y. Lee, Composite properties of calcium-based alkali-activated slag composites reinforced by different types of polyethylene fibers and micromechanical analysis, Construction and Building Materials 273 (2021) 121760.

[11] Z. Giergiczny, Fly ash and slag, Cement and Concrete Research 124 (2019) 105826.

[12] S. Zhang, E. Duque-Redondo, A. Kostiuchenko, J.S. Dolado, G. Ye, Molecular dynamics and experimental study on the adhesion mechanism of polyvinyl alcohol (PVA) fiber in alkali-activated slag/fly ash, Cement and Concrete Research 145 (2021) 106452.

[13] B. Nematollahi, J. Sanjayan, J. Qiu, E.-H. Yang, Micromechanics-based investigation of a sustainable ambient temperature cured one-part strain hardening geopolymer composite, Construction and Building Materials 131 (2017) 552-563.

[14] G. Fang, W.K. Ho, W. Tu, M. Zhang, Workability and mechanical properties of alkali-activated fly ash-slag concrete cured at ambient temperature, Construction and Building Materials 172 (2018) 476-487.

[15] Y. Wang, C.L. Chan, S.H. Leong, M. Zhang, Engineering properties of strain hardening geopolymer composites with hybrid polyvinyl alcohol and recycled steel fibres, Construction and Building Materials 261 (2020) 120585.

[16] Y. Wang, Y. Wang, M. Zhang, Effect of sand content on engineering properties of fly ash-slag based strain hardening geopolymer composites, Journal of Building Engineering 34 (2021) 101951.

[17] H. Zhong, M. Zhang, Effect of recycled tyre polymer fibre on engineering properties of sustainable strain hardening geopolymer composites, Cement and Concrete Composites 122 (2021) 104167.
[18] B. Nematollahi, J. Sanjayan, J. Qiu, E.-H. Yang, High ductile behavior of a polyethylene fiber-reinforced one-part geopolymer composite: A micromechanics-based investigation, Archives of Civil and Mechanical Engineering 17(3) (2017) 555-563.
[19] L. Kan, F. Wang, Z. Zhang, W. Kabala, Y. Zhao, Mechanical properties of high ductile alkali-activated fiber reinforced composites with different curing ages, Construction and Building Materials 306 (2021) 124833.
[20] S. Zhang, V.C. Li, G. Ye, Micromechanics-guided development of a slag/fly ash-based strain-hardening geopolymer composite, Cement and Concrete Composites 109 (2020) 103510.
[21] Y. Ling, K. Wang, W. Li, G. Shi, P. Lu, Effect of slag on the mechanical properties and bond strength of fly ash-based engineered geopolymer composites, Composites Part B: Engineering 164 (2019) 747-757.
[22] M. Farooq, A. Krishna, N. Banthia, Highly ductile fiber reinforced geopolymers under tensile impact, Cement and Concrete Composites 126 (2022) 104374.
[23] J. Yu, H.-L. Wu, C.K.Y. Leung, Feasibility of using ultrahigh-volume limestone-calcined clay blend to develop sustainable medium-strength Engineered Cementitious Composites (ECC), Journal of Cleaner Production 262 (2020) 121343.
[24] D. Zhang, J. Yu, H. Wu, B. Jaworska, B.R. Ellis, V.C. Li, Discontinuous micro-fibers as intrinsic reinforcement for ductile Engineered Cementitious Composites (ECC), Composites Part B: Engineering 184 (2020) 107741.
[25] J. Yu, C.K. Leung, Strength improvement of strain-hardening cementitious composites with ultrahigh-volume fly ash, Journal of Materials in Civil Engineering 29 (2017) 05017003.
[26] R. Merli, M. Preziosi, A. Acampora, M.C. Lucchetti, E. Petrucci, Recycled fibers in reinforced concrete: A systematic literature review, Journal of Cleaner Production 248 (2019) 119207.
[27] K.M. Liew, A. Akbar, The recent progress of recycled steel fiber reinforced concrete, Construction and Building Materials 232 (2020) 117232.
[28] J. Yu, J. Yao, X. Lin, H. Li, J.Y.K. Lam, C.K.Y. Leung, I.M.L. Sham, K. Shih, Tensile performance of sustainable Strain-Hardening Cementitious Composites with hybrid PVA and recycled PET fibers, Cement and Concrete Research 107 (2018) 110-123.
[29] G. Malarvizhi, N. Senthul, C. Kamaraj, A study on Recycling of crumb rubber and low density polyethylene blend on stone matrix asphalt, International Journal of Science and Research 2(10) (2012).

[30] J. Qiu, H.S. Tan, E.-H. Yang, Coupled effects of crack width, slag content, and conditioning alkalinity on autogenous healing of engineered cementitious composites, Cement and Concrete Composites 73 (2016) 203-212.

[31] A.C.C. Trindade, A.A. Heravi, I. Curosu, M. Liebscher, F. de Andrade Silva, V. Mechtcherine, Tensile behavior of strain-hardening geopolymer composites (SHGC) under impact loading, Cement and Concrete Composites 113 (2020) 103703.

[32] J. Cai, J. Pan, J. Han, Y. Lin, Z. Sheng, Low-energy impact behavior of ambient cured engineered geopolymer composites, Ceramics International (2021).

[33] J. Cai, J. Pan, J. Han, Y. Lin, Z. Sheng, Impact behaviours of engineered geopolymer composite exposed to elevated temperatures, Construction and Building Materials 312 (2021) 125421.

[34] ASTM C618-17a, Standard Specification for Coal Fly Ash and Raw or Calcined Natural Pozzolan for Use in Concrete, ASTM International, West Conshohocken, PA, 2017.

[35] M. Chen, H. Zhong, M. Zhang, Flexural fatigue behaviour of recycled tyre polymer fibre reinforced concrete, Cement and Concrete Composites 105 (2020) 103441.

[36] O. Onuaguluchi, N. Banthia, Durability performance of polymeric scrap tire fibers and its reinforced cement mortar, Materials and Structures 50(2) (2017).

[37] M. Chen, H. Zhong, L. Chen, Y. Zhang, M. Zhang, Engineering properties and sustainability assessment of recycled fibre reinforced rubberised cementitious composite, Journal of Cleaner Production 278 (2021) 123996.

[38] ASTM C1437-15, Standard Test Method for Flow of Hydraulic Cement Mortar, ASTM International, West Conshohocken, PA, United States, 2015.

[39] ASTM C39/39M-21, Standard Test Method for Compressive Strength of Cylindrical Concrete Specimens, ASTM International, West Conshohocken, PA, United States, 2021.

[40] Wang, Shasha, Zhang, Min-Hong, Quek, Ser, T.J.J.o. Testing, Evaluation, Effect of Specimen Size on Static Strength and Dynamic Increase Factor of High-Strength Concrete from SHPB Test, (2011).

[41] J. Xiao, L. Li, L. Shen, C.S. Poon, Compressive behaviour of recycled aggregate concrete under impact loading, Cement and Concrete Research 71 (2015) 46-55.

[42] M.Z.N. Khan, Y. Hao, H. Hao, F.U.A. Shaikh, Experimental evaluation of quasi-static and dynamic compressive properties of ambient-cured high-strength plain and fiber reinforced geopolymer composites, Construction and Building Materials 166 (2018) 482-499.

[43] ASTM C469, Standard Test Method for Static Modulus of Elasticity and Poisson's Ratio of Concrete in Compression, ASTM International, West Conshohocken, PA, United States, 2014.

[44] L.D. Bertholf, C.H. Karnes, Two-dimensional analysis of the split hopkinson pressure bar system, Journal of the Mechanics and Physics of Solids 23(1) (1975) 1-19.

[45] W. W. Chen, B. Song, Split Hopkinson (Kolsky) Bar: Design, Testing and Applications, 2011.

[46] Q. Yu, W. Zhuang, C. Shi, Research progress on the dynamic compressive properties of ultra-high performance concrete under high strain rates, Cement and Concrete Composites 124 (2021).

[47] B.A. Gama, S.L. Lopatnikov, J.W. Gillespie Jr, Hopkinson bar experimental technique: a critical review, J Appl. Mech. Rev. 57(4) (2004) 223-250.

[48] A. Bagher Shemirani, R. Naghdabadi, M.J. Ashrafi, Experimental and numerical study on choosing proper pulse shapers for testing concrete specimens by split Hopkinson pressure bar apparatus, Construction and Building Materials 125 (2016) 326-336.

[49] B. Huang, Y. Xiao, Compressive impact tests of lightweight concrete with 155-mm-diameter spilt hopkinson pressure bar, Cement and Concrete Composites 114 (2020) 103816.

[50] S. Jiang, B. Shan, J. Ouyang, W. Zhang, X. Yu, P. Li, B. Han, Rheological properties of cementitious composites with nano/fiber fillers, Construction and Building Materials 158 (2018) 786-800.

[51] N. Ranjbar, M. Zhang, Fiber-reinforced geopolymer composites: A review, Cement and Concrete Composites 107 (2020) 103498.

[52] G. Masi, W.D.A. Rickard, M.C. Bignozzi, A. van Riessen, The effect of organic and inorganic fibres on the mechanical and thermal properties of aluminate activated geopolymers, Composites Part B: Engineering 76 (2015) 218-228.

[53] V. Afroughsabet, L. Biolzi, P.J.M. Monteiro, The effect of steel and polypropylene fibers on the chloride diffusivity and drying shrinkage of high-strength concrete, Composites Part B: Engineering 139 (2018) 84-96.

[54] H. Zhong, M. Zhang, Experimental study on engineering properties of concrete reinforced with hybrid recycled tyre steel and polypropylene fibres, Journal of Cleaner Production 259 (2020) 120914.

[55] K. Yu, Y. Ding, Y.X. Zhang, Size effects on tensile properties and compressive strength of engineered cementitious composites, Cement and Concrete Composites 113 (2020) 103691.

[56] J.-X. Lin, Y. Song, Z.-H. Xie, Y.-C. Guo, B. Yuan, J.-J. Zeng, X. Wei, Static and dynamic mechanical behavior of engineered cementitious composites with PP and PVA fibers, Journal of Building Engineering 29 (2020) 101097.

[57] L.-l. Kan, W.-s. Wang, W.-d. Liu, M. Wu, Development and characterization of fly ash based PVA fiber reinforced Engineered Geopolymer Composites incorporating metakaolin, Cement and Concrete Composites 108 (2020) 103521.

[58] M. Chen, H. Zhong, H. Wang, M. Zhang, Behaviour of recycled tyre polymer fibre reinforced concrete under dynamic splitting tension, Cement and Concrete Composites 114 (2020) 103764.

[59] A. Baričević, M. Jelčić Rukavina, M. Pezer, N. Štirmer, Influence of recycled tire polymer fibers on concrete properties, Cement and Concrete Composites 91 (2018) 29-41.

[60] M.Z.N. Khan, Y. Hao, H. Hao, F.U.A. Shaikh, Mechanical properties of ambient cured high strength hybrid steel and synthetic fibers reinforced geopolymer composites, Cement and Concrete Composites 85 (2018) 133-152.

[61] N. Ganesan, P.V. Indira, A. Santhakumar, Engineering properties of steel fibre reinforced geopolymer concrete, Advances in concrete construction 1(4) (2013) 305-318.

[62] ACI 318, Building Code Requirements for Structural Concrete and Commentary American Concrete Institute, 2008.

[63] CEB-FIP model code 1990: Design code, Comite Euro-Inernational Du Beton 1990.

[64] N.K. Lee, H.K. Lee, Setting and mechanical properties of alkali-activated fly ash/slag concrete manufactured at room temperature, Construction and Building Materials 47 (2013) 1201-1209.

[65] B. Nematollahi, J. Sanjayan, F.U.A. Shaikh, Matrix design of strain hardening fiber reinforced engineered geopolymer composite, Composites Part B: Engineering 89 (2016) 253-265.

[66] N. Li, Z. Jin, G. Long, L. Chen, Q. Fu, Y. Yu, X. Zhang, C. Xiong, Impact resistance of steel fiber-reinforced self-compacting concrete (SCC) at high strain rates, Journal of Building Engineering 38 (2021) 102212.

[67] T.M. Pham, W. Chen, A.M. Khan, H. Hao, M. Elchalakani, T.M. Tran, Dynamic compressive properties of lightweight rubberized concrete, Construction and Building Materials 238 (2020) 117705.

[68] Y. Hao, H. Hao, Dynamic compressive behaviour of spiral steel fibre reinforced concrete in split Hopkinson pressure bar tests, Construction and Building Materials 48 (2013) 521-532.

[69] X. Chen, S. Wu, J. Zhou, Experimental and modeling study of dynamic mechanical properties of cement paste, mortar and concrete, Construction and Building Materials 47 (2013) 419-430.

[70] G.M. Ren, H. Wu, Q. Fang, J.Z. Liu, Effects of steel fiber content and type on dynamic compressive mechanical properties of UHPCC, Construction and Building Materials 164 (2018) 29-43.

[71] Q. Fu, D. Niu, J. Zhang, D. Huang, M. Hong, Impact response of concrete reinforced with hybrid basalt-polypropylene fibers, Powder Technology 326 (2018) 411-424.

[72] C. Wang, W. Chen, H. Hao, S. Zhang, R. Song, X. Wang, Experimental investigations of dynamic compressive properties of roller compacted concrete (RCC), Construction and Building Materials 168 (2018) 671-682.

[73] S.-H. Xiao, S.-J. Liao, G.-Q. Zhong, Y.-C. Guo, J.-X. Lin, Z.-H. Xie, Y. Song, Dynamic properties of PVA short fiber reinforced low-calcium fly ash - slag geopolymer under an SHPB impact load, Journal of Building Engineering 44 (2021).

[74] Z. Wu, C. Shi, W. He, D. Wang, Static and dynamic compressive properties of ultra-high performance concrete (UHPC) with hybrid steel fiber reinforcements, Cement and Concrete Composites 79 (2017) 148-157.

[75] A.B. Groeneveld, T.M. Ahlborn, C.K. Crane, C.A. Burchfield, E.N. Landis, Dynamic strength and ductility of ultra-high performance concrete with flow-induced fiber alignment, International Journal of Impact Engineering 111 (2018) 37-45.

[76] H. Huang, X. Gao, K.H. Khayat, Contribution of fiber orientation to enhancing dynamic properties of UHPC under impact loading, Cement and Concrete Composites 121 (2021) 104108.

[77] Y. Hao, H. Hao, G.P. Jiang, Y. Zhou, Experimental confirmation of some factors influencing dynamic concrete compressive strengths in high-speed impact tests, Cement and Concrete Research 52 (2013) 63-70.

[78] J. Lai, W. Sun, Dynamic behaviour and visco-elastic damage model of ultra-high performance cementitious composite, Cement and Concrete Research 39(11) (2009) 1044-1051.

[79] W. Ren, J. Xu, J. Liu, H. Su, Dynamic mechanical properties of geopolymer concrete after water immersion, Ceramics International 41(9, Part B) (2015) 11852-11860.

[80] M. Zhang, H.J. Wu, Q.M. Li, F.L. Huang, Further investigation on the dynamic compressive strength enhancement of concrete-like materials based on split Hopkinson pressure bar tests. Part I: Experiments, International Journal of Impact Engineering 36(12) (2009) 1327-1334.

[81] Q. Fu, Z. Zhang, X. Zhao, M. Hong, B. Guo, Q. Yuan, D. Niu, Water saturation effect on the dynamic mechanical behaviour and scaling law effect on the dynamic strength of coral aggregate concrete, Cement and Concrete Composites 120 (2021).

[82] B. Zhang, Y. Feng, J. Xie, J. He, Y. Zhang, C. Cai, D. Huang, L. Li, Effects of fibres on ultra-lightweight high strength concrete: Dynamic behaviour and microstructures, Cement and Concrete Composites 128 (2022) 104417.

[83] C. Redon, V. Li, C. Wu, H. Hoshiro, T. Saito, A. Ogawa, Measuring and Modifying Interface Properties of PVA Fibers in ECC Matrix, 2001.

[84] W.P. Boshoff, V. Mechtcherine, G.P.A.G. van Zijl, Characterising the time-dependant behaviour on the single fibre level of SHCC: Part 1: Mechanism of fibre pull-out creep, Cement and Concrete Research 39(9) (2009) 779-786.

[85] E.-H. Yang, V.C. Li, Strain-rate effects on the tensile behavior of strain-hardening cementitious composites, Construction and Building Materials 52 (2014) 96-104.

[86] I. Curosu, V. Mechtcherine, O. Millon, Effect of fiber properties and matrix composition on the tensile behavior of strain-hardening cement-based composites (SHCCs) subject to impact loading, Cement and Concrete Research 82 (2016) 23-35.

[87] M. Serdar, A. Baričević, M. Jelčić Rukavina, M. Pezer, D. Bjegović, N. Štirmer, Shrinkage Behaviour of Fibre Reinforced Concrete with Recycled Tyre Polymer Fibres, International Journal of Polymer Science 2015 (2015) 1-9.

[88] L. Yang, X. Lin, R.J. Gravina, Evaluation of dynamic increase factor models for steel fibre reinforced concrete, Construction and Building Materials 190 (2018) 632-644.

[89] S. Wang, M.-H. Zhang, S.T. Quek, Effect of high strain rate loading on compressive behaviour of fibre-reinforced high-strength concrete, 63(11) (2011) 813-827.

[90] FIB Model Code for Concrete Structures 2010, Comite Euro-Inernational Du Beton 2013.

[91] P.H. Bischoff, S.H. Perry, Compressive behaviour of concrete at high strain rates, Materials and Structures 24(6) (1991) 425-450.

[92] Y. Su, J. Li, C. Wu, P. Wu, Z.-X. Li, Influences of nano-particles on dynamic strength of ultra-high performance concrete, Composites Part B: Engineering 91 (2016) 595-609.

[93] X. Zhao, Q. Li, S. Xu, Contribution of steel fiber on the dynamic tensile properties of hybrid fiber ultra high toughness cementitious composites using Brazilian test, Construction and Building Materials 246 (2020) 118416.

[94] C. Lu, J. Yu, C.K.Y. Leung, Tensile performance and impact resistance of Strain Hardening Cementitious Composites (SHCC) with recycled fibers, Construction and Building Materials 171 (2018) 566-576.

The authors declare that they have no known competing financial interests or personal relationships that could have appeared to influence the work reported in this paper.